Pulsed-Field Gradient Nuclear Magnetic Resonance as a Tool for Studying Translational Diffusion: Part II. Experimental Aspects

WILLIAM S. PRICE

Water Research Institute, Sengen 2-1-6, *Tsukuba, Ibaraki* 305-0047, *Japan; E-mail: wprice@wri.co.jp*

ABSTRACT: In Part 1 of this series, we considered the theoretical basis behind the pulsed-field gradient nuclear magnetic resonance method for measuring diffusion. In this article the experimental and practical aspects of conducting such experiments are considered, including technical problems involved in gradient production such as eddy currents, gradient calibration, internal gradients in heterogeneous samples, and temperature control. Furthermore, the means for recognizing and preventing or at least minimizing these problems are discussed. A number of representative pulse sequences are also reviewed.
© 1998 John Wiley & Sons, Inc. Concepts Magn Reson 10: 197–237, 1998

KEY WORDS: background gradient; diffusion; eddy currents; gradient calibration; pulsed field gradient

INTRODUCTION: PERFORMING A SIMPLE PULSED-FIELD GRADIENT (PFG) NUCLEAR MAGNETIC RESONANCE (NMR) MEASUREMENT

In the first article (*1*) of this series (referred to here as Part 1) on PFG NMR [aso known as pulsed-gradient spin-echo (PGSE) NMR] diffusion measurements, we considered in detail the underlying principles of the PFG NMR experiment (Figure 1) and presented the basic mathematical analysis required to analyze the results of such experiments. This article expands the first one by considering the experimental aspects and complications.

Let us begin by assuming that we have a simple liquid sample such as H_2O or CCl_4 where there is only one species, and that we wish to measure its diffusion coefficient, D, using the simple Hahn spin-echo–based PFG pulse sequence (i.e., the Stejskal and Tanner sequence)

Received 12 December 1997; revised 5 February 1998; accepted 6 February 1998.

Concepts in Magnetic Resonance, Vol. 10(4) 197–237 (1998)
© 1998 John Wiley & Sons, Inc. CCC 1043-7347/98/040197-41

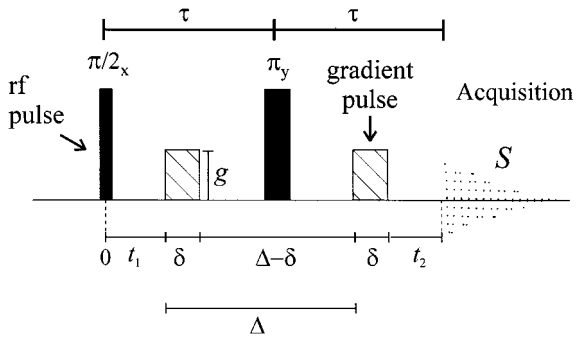

Figure 1 The Stejskal and Tanner pulsed-field gradient NMR sequence. The principles of this sequence for measuring diffusion were presented in Part 1. This is the simplest pulse sequence for measuring diffusion. Phase cycling can be included to remove spectrometer artifacts. We have indicated the second half of the echo by dots, as it is this part of the echo (i.e., starting at $t = 2\tau$) that is digitized and used as the FID.

shown in Fig. 1. To perform this sequence, the spectrometer must be equipped with a current amplifier, under software control, which can send current pulses to a gradient coil placed around the sample (Fig. 2). Since this simple sequence is based on a Hahn spin-echo, the echo signal, S, is attenuated by both the effects of the spin–spin relaxation and of diffusion. As shown in Part 1 (*1*), the signal intensity is given by

$$S(2\tau) = S(0)\underbrace{\exp\left(\frac{-2\tau}{T_2}\right)}_{\text{attenuation due to relaxation}} \times \underbrace{\exp(-\gamma^2 g^2 D\delta^2(\Delta - \delta/3))}_{\text{attenuation due to diffusion}} = S(2\tau)_{g=0}\exp(-\gamma^2 g^2 D\delta^2(\Delta - \delta/3)) \quad [1]$$

where $S(0)$ is the signal immediately after the $\pi/2$ pulse, 2τ is the total echo time, T_2 is the spin–spin relaxation time of the species, γ is the gyromagnetic ratio of the observe nucleus, g is the strength of the applied gradient, and δ and Δ are the duration of the gradient pulses and the separation between them, respectively. Typically, δ is in the range of 0–10 ms, Δ is in the range of milliseconds to seconds and g is up to 20 T m^{-1}. To remove the effects of the signal attenuation due to, in the case of the Stejskal and Tanner sequence, spin–spin relaxation, we normalize the signal with respect to the signal obtained in the absence of the applied gradient and thereby define the echo attenuation to be

$$E(2\tau) = \frac{S(2\tau)_{g=0}\exp(-\gamma^2 g^2 D\delta^2(\Delta - \delta/3))}{S(2\tau)_{g=0}} = \exp(-\gamma^2 g^2 D\delta^2(\Delta - \delta/3)) \quad [2]$$

By inspection of Eq. [2] with reference to Fig. 1, it can be seen that to measure diffusion, a series of experiments are performed in which either g, δ, or Δ is varied while keeping τ constant. Then, Eq. [2] is regressed onto the experimental data and D is straightforwardly determined as discussed in Part 1.

Unfortunately, the above description pertains only to performing the diffusion measurements under ideal conditions, and includes the following implicit assumptions: (a) the gradient pulses are perfectly rectangular (i.e., infinitely fast rise and fall times), (b) the gradient pulses are equally matched and of known strength, (c) the only magnetic field gradients present are the applied gradient pulses, (d) all of the sample is subject to exactly the same gradient, (e) all of the sample is at exactly the same temperature, and (f) the relaxation characteristics of the sample do not constrain the choice of Δ or the recycle time of the pulse sequence. In a real experiment, all of these points must be addressed, or at least their significance understood. These points are considered in this article.

Although few researchers will attempt to construct their own equipment since the requisite gradient hardware is now commercially available, a basic understanding of gradient pulse generation provides valuable insight into spectrometer limitations and related problems. Accordingly, in the next section we will briefly consider the hardware required to generate magnetic-field gradient pulses and what levels of performance are required for conducting diffusion experiments. Hardware problems and the experimental ramifications of imperfect gradient pulses will be considered in the third section. Sample preparation and spectrometer setup will be considered in the fourth section. Problems relating directly to the sample and their solutions are discussed in the fifth section. In the penultimate section, the methods for calibrating the applied gradient are considered; and finally, in the last section, a summary of how to conduct PFG experiments is presented. As in our previous article, we will confine ourselves to the more commonly used PFG exper-

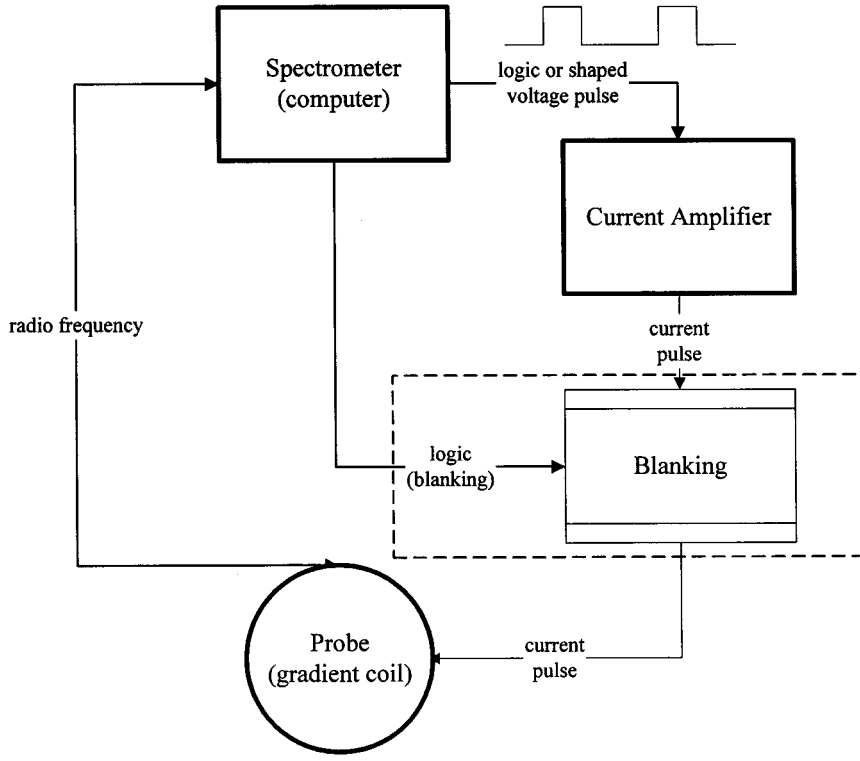

Figure 2 A schematic diagram of the components necessary to perform pulsed-field gradient NMR and their relationship to the rest of the spectrometer. At the appropriate points in the pulse sequence, the spectrometer sends logic pulses or (on more sophisticated machines) shaped voltage pulses (waveforms) such as trapezoidal pulses or pulses with pre-emphasis to the current amplifier. The current amplifier is, in turn, connected to the gradient coils placed around the sample in the probe head (Fig. 4). Sophisticated hardware will also allow the polarity of the gradient pulses to be specified, thus affording the possibility of performing pulse sequences with bipolar gradient pulses. More advanced spectrometers also include current blanking circuitry which prevents earth loops and thereby helps to minimize background gradients. In this case, the current pulse circuitry is blanked out between gradient pulses.

iments based on magnetic field (i.e., B_0) gradients. It is appropriate to mention that many of the complications that affect PFG measurements also apply to imaging experiments; consequently, some of the solutions to the technical problems were developed with imaging in mind (2).

HARDWARE

Introduction

The hardware aspects of PFG NMR have been discussed by a number of authors (e.g., Refs. *2–7*), and for the present purposes it is sufficient to provide a basic overview. The additional hardware that must be added to a spectrometer to generate gradient pulses is summarized in Fig. 2. Specifically, the spectrometer, in accordance with the pulse sequence, needs to output either a logic pulse (if only rectangular pulses are required) or a shaped voltage pulse (thereby affording the possibility of shaped gradient pulses) to an amplifier. Ideally, the polarity of the gradient pulse will also be able to be specified. In turn, the amplifier outputs a corresponding current pulse to the gradient coil.

Gradient Coils

Many gradient coil designs exist (see Refs. *6–8*); however, we will restrict our discussion to the simplest commonly used geometry for producing gradients along the z direction in superconducting magnets: the Maxwell pair of coils (i.e., anti-Helmholtz) [Fig. 3(A)]. The magnetic field strength at a point $P = (r_p, z_p)$ (Fig. 3) from a single

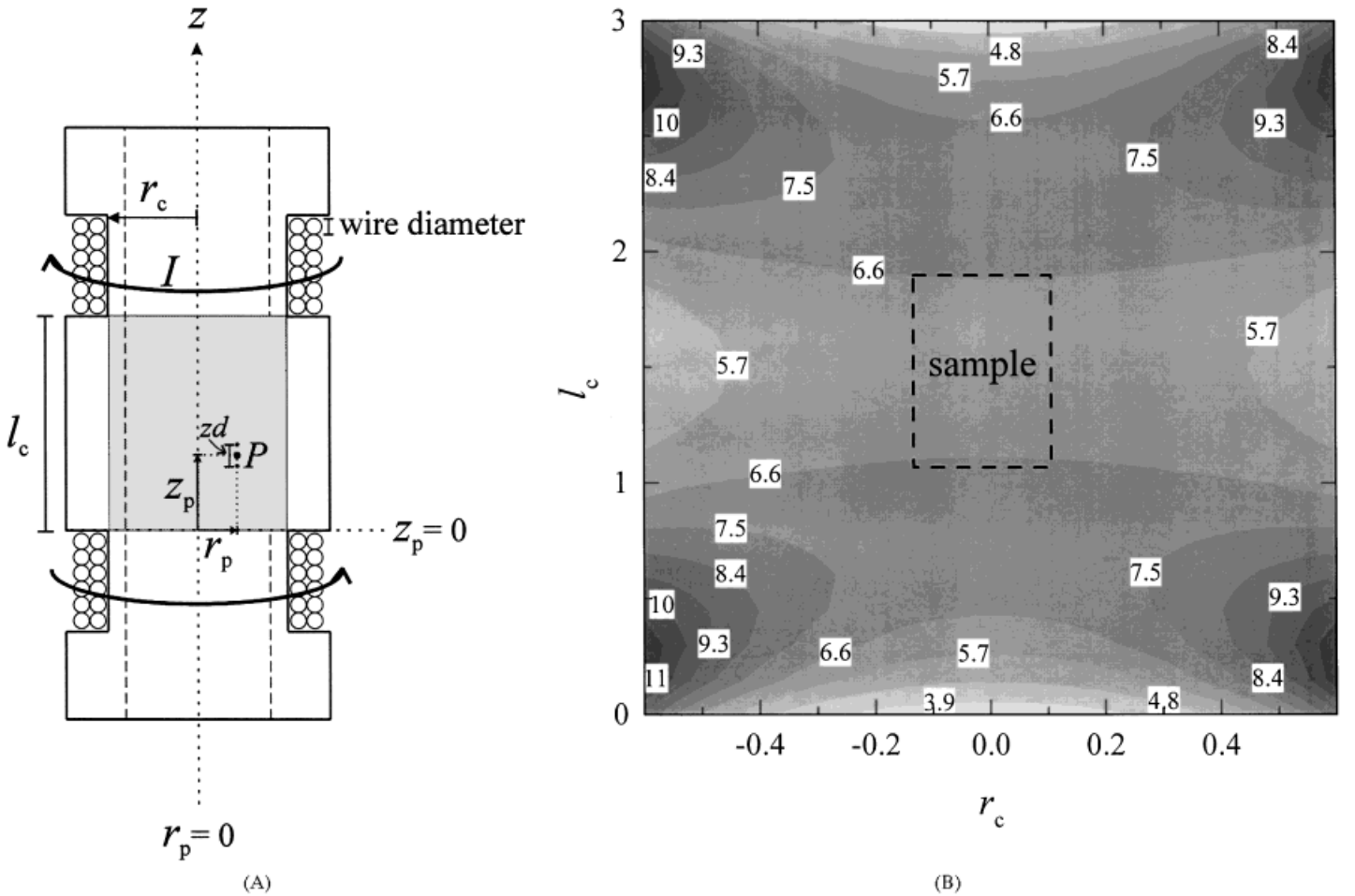

FIGURE 3 (A) A schematic depiction of a cross-section through a Maxwell pair; this is a gradient coil for producing a gradient along the long axis of the coil and is the basis of most gradient coils for producing z-axis gradients in superconducting magnets. It should be noted that each set of windings has an opposite handedness. In computing the gradient using Eqs. [3] and [4], the coil radius r_c is adjusted according to the actual winding being calculated. The gradient g_z at a point P is calculated by computing the magnetic field at two points separated by a distance along the z axis, zd, (i.e., $P_1 = (r_p, z_p + zd/2)$ and $P_2 = (r_p, z_p - zd/2)$, denoted by the smaller solid circles) and dividing by the distance between them. (B) A contour plot of the gradient in the shaded region of the gradient coil depicted in (A) taking r_c to be 0.6 cm, l_c to be 3 cm, the wire diameter to be 0.5 mm, and $I = 1$ A. The numbers on the contours denote the gradient strength in G cm^{-1} (n.b., 1 G cm^{-1} = 0.01 T m^{-1}). Because this is a very simplistic design for a gradient coil, the volume having a constant (i.e., linear) gradient is very small. Ideally, the sample would be restricted to a volume with high gradient linearity (e.g., the dashed box).

winding can be estimated from the Biot–Savart law (*9*, *10*),

$$B_0(r_p, z_p) = \frac{\mu_0 I}{2\pi} \frac{1}{\left((r_c + r_p)^2 + z_p^2\right)^{1/2}} \times \left\{ K(u) + \frac{r_c^2 - r_p^2 - z_p^2}{(r_c - r_p)^2 + z_p^2} E(u) \right\} \quad [3]$$

where

$$u = \sqrt{\frac{4 r_c r_p}{(r_c + r_p)^2 + z_p^2}}$$

K and E are the elliptic integrals of the first and second kinds, respectively (*11*). μ_0 is the permitivity constant, r_p is the radius of the point at which the gradient is calculated, r_c is the radius of the gradient coil, and z_p is the displacement along the z axis from the coil (Fig. 3). The gradient at P can then be computed by calculating the magnetic field strength at two points separated by a distance along the z axis, zd (i.e., $P_1 = (r_p, z_p + zd/2)$, and $P_2 = (r_p, z_p - zd/2)$), and dividing by the distance between the two points,

$$g_{z,P} = \frac{\sum_{\substack{\text{coil} \\ \text{windings}}} \left[B_0\left(r_p, z_p + \frac{zd}{2}\right) - B_0\left(r_p, z_p - \frac{zd}{2}\right) \right]}{zd} \quad [4]$$

In calculating Eq. [4], it must be remembered that the sum runs over both windings of the Maxwell pair, and owing to the opposite polarity, one coil winding is taken as negative. Ideally, the gradient coils should produce a perfectly constant (or commonly termed "linear") gradient, but owing to the space constraints inside the probe and inherent limitations in construction, such as attempting to produce a continuous magnetic field distribution from a finite number of turns [Fig. 3(A)], the gradient coils never produce a perfectly constant gradient. A field plot for the gradient coils depicted in Fig. 3(A) is given in Fig. 3(B).

As will be explained in more detail below (see Eddy Currents and Perturbation of B_0), disturbances can result from the generation of eddy currents in the conductors surrounding the gradient coils owing to the rapid pulsing of the gradient coils. The most direct solution to this problem is to limit the effects of the gradient pulse to the sample volume only. This is achieved by placing a shield gradient coil outside the (primary) gradient coil (Fig. 4). Shielded gradient coils were originally proposed by Mansfield and Chapman (*12*, *13*), Turner (*14*), and Turner and Bowley (*15*), and the theoretical aspects of shielded gradient coils have recently been summarized elsewhere (*2*, *16*). The shield coil is designed to prevent (i.e., cancel) the effects of the gradient pulse generated by the primary gradient coil radiating outward. Ideally, the change in the magnetic field outside the gradient set due to the pulse would be zero, whereas the gradient generated in the sample volume would be unaffected by the presence of the shield coil. In this way, no (or at least greatly reduced) eddy currents are generated, typically to $< 1\%$ (*17*). We also note that these eddy current effects rapidly attenuate with increasing distance, and thus there is considerable advantage in using small field gradient coils in a wide-bore magnet. Importantly, after implementation, shielded gradient coils require no further experimental adjustment. A negative aspect of shielded gradient coils is that the shield coils decrease the strength and linearity of the gradient produced by the primary gradient coil (*18*). It is possible to generate a profile of the gradient strength by applying a read gradient during acquisition in the PFG sequence (*19*) (this is related to the one-dimensional imaging method of calibrating the gradient strength discussed in Shape Analysis of the Spin Echo and One-Dimensional Images but retaining the gradient pulses for measuring diffusion). However, it has been found in practice that a reasonable deviation from perfect linearity is allowable for many experiments (*20*). A simple but tedious experimental means of testing the linearity of the gradient is to perform diffusion measurements using a very small sample at different positions within the volume where the sample would normally lie. A water sample in a small spherical bulb (e.g., Wilmad cat. no. 529A) is a convenient choice.

Although most diffusion studies are performed with a gradient in one dimension only, it is now increasingly common, especially with the advent of imaging and microscopy probes, to perform diffusion experiments in three dimensions so as

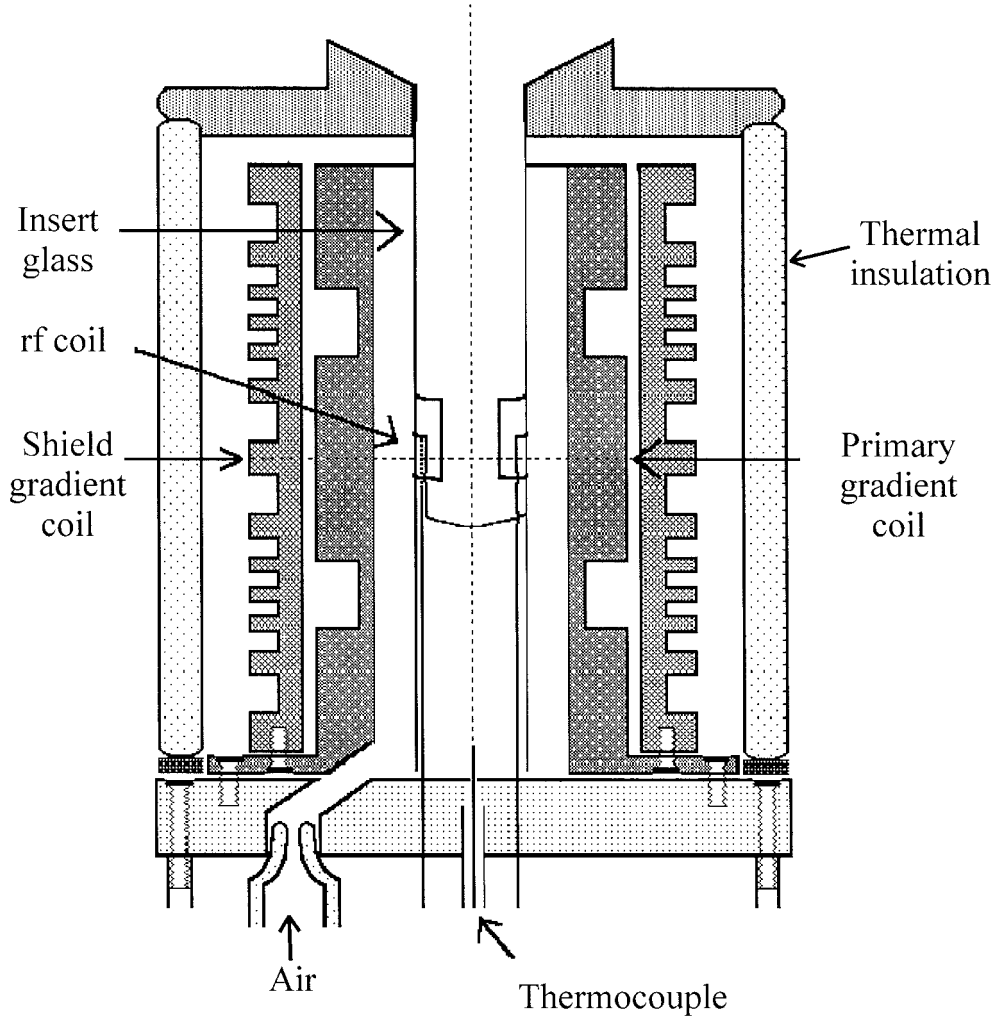

Figure 4 An example of a shielded magnetic gradient coil system in an NMR probe head. Only the coil formers are shown, and the wires can be imagined to be wound around the slots on the formers. The primary gradient coil produces the constant gradient over the sample volume which is contained within the rf coils. The shield coil is designed to prevent the gradient pulse from affecting outside the gradient coils, thereby preventing the generation of eddy currents [adapted from Price et al. (*6*)]. In very high gradient systems, the actual gradient coils must be air or water cooled. The position of the thermocouple is critical for the accuracy and stability of the temperature control. The inclusion of gradient coils in the probe head normally makes the probe more difficult to shim.

to obtain the diffusion tensor (see Part 1, Anisotropic Diffusion).

Amplifiers

Ideally, we desire infinitely fast rise and fall times of the gradient pulses. In practice, there are two factors which limit the maximum current switching speed; the first is that the power supply voltage must equal $RI + L\,dI/dt$, where I is the current and L and R are the load (i.e., gradient coils plus leads) inductance and resistance, respectively, and the second is the slew rate (i.e., the maximum rate of change of the output voltage) of the power supply. Thus, the amplifier used must have suitable current and voltage parameters to drive the gradient coil used. Typically rise and fall times of the gradient pulses are on the order of 50 μs.

Since the current through a gradient coil induces heating, which in turn results in a change in gradient coil resistance, the amplitude of the gra-

dient pulses might change during the sequence. In fact, many gradient coils, especially when used with large currents or duty cycles, need to be air and/or water cooled to prevent physical damage. Similarly, in conducting variable temperature diffusion measurements, the gas used for heating and cooling the sample will also have some effect on the gradient coil temperature. The use of a constant current supply, instead of a constant voltage amplifier, obviates the need to calibrate the gradient for each sample temperature or particular experimental parameters. The negative aspects of a constant current amplifier are that it is difficult to achieve very low noise figures and rapid settling.

HARDWARE PROBLEMS AND SOLUTIONS

Sample Movement with Respect to the Gradient

Mechanical stability is extremely important, since movements on the order of 10 nm will restrict diffusion measurements to $D \geq 10^{-15}$ m^2s^{-1} (*21*) (e.g., see Part 1, Eq. [33], and consider the mean square displacement that occurs with such a diffusion coefficient and a typical value of Δ such as 50 ms). Sample movement is similar to flow in that all spins in the case of a rigid sample receive an equal phase shift (as in the case of flow; see Part 1, Measuring Diffusion with Magnetic Field Gradients) instead of a phase twist. Thus, assuming that the sample moves by $\Delta\mathbf{r}$ between the first and second gradient pulses of strength $\mathbf{g}$ and duration δ, then the net phase shift would be given by

$$\begin{aligned}\phi_{\text{movement}} &= \exp(i\gamma\delta\mathbf{g}\cdot\Delta\mathbf{r}) \\ &= \exp(i2\pi\mathbf{q}\cdot\Delta\mathbf{r}) \qquad [5]\end{aligned}$$

where $\mathbf{q} = (2\pi)^{-1}\gamma\delta\mathbf{g}$.

A string of equally spaced (i.e., by Δ) gradient pulses before the start of the pulse sequence may also help to alleviate motional disturbances during the encoding and decoding gradient pulses (*22*) (see Fig. 8). Sample movement or vibration can result in greatly increased echo attenuation (*23*) and attenuation plots containing artifactual diffraction minima; however, these artifactual diffractive minima are evident at even modest attenuations, whereas real diffractive minima (see Part 1, especially Fig. 8) generally do not become evident until the echo signal has been attenuated by nearly two orders of magnitude. To check for the possibility of vibration, it is advisable to perform a measurement under the same conditions to be used experimentally with a very large monodisperse polymer (e.g., polydimethylsiloxane, MW $\sim$ 700 000 has a diffusion coefficient below 10^{-15} m^2s^{-1} (*24*)) for which true diffractive peaks cannot occur and for which the diffusion coefficient is generally below the limits of measurability (*25*). If, assuming that the sample is correctly positioned in the probe, no attenuation is observed, the presence of artifacts can be excluded. However, this test does not account for independent movement of the sample with respect to the sample tube as might occur with a powder sample (e.g., zeolite) (*23*). In such cases, the samples may need to be specially compacted into the NMR tube (*23*). If the measured diffusion coefficient is observed to be observation time independent (although Δ must be sufficiently small so that the effects of restricted diffusion are insignificant), artifacts due to sample instability can be excluded.

Radiofrequency (rf) Coupling

The addition of gradient coils to an NMR probe generally has a deleterious effect on general probe performance. Although with modern commercially obtainable equipment this is becoming less of an issue, we mention the effects here for completeness. Partly owing to the proximity of the gradient coils to the sample region, the gradient coils and leads have the possibility of acting as antennae and introducing rf interference. In fact, the present author has also observed the heater cable to be a source of rf interference. The presence of rf interference can be tested for by observing a spectrum—for example, after a $\pi/2$ pulse—and then disconnecting the gradient current leads and acquiring another spectrum. The rf interference will appear as spikes and/or general noise. It has been the present author's experience that frequencies below 200 MHz are more problematic for this kind of interference. Apart from simply collecting a far greater number of scans to obtain sufficient signal-to-noise, the best solution is to employ rf filtering on these sources of interference. A related problem is the possible strong mutual inductance between the gradient and the rf coils. Thus, the Q of the rf coil(s) are diminished, resulting in longer $\pi/2$ pulses, poorer decoupling efficiency, and a poorer signal-to-noise ratio.

Amplifier Noise, Earth Loops, and Nonreproducible (Mismatched) Gradient Pulses

In this section, we consider the effects introduced by unintended currents flowing through the gradient system resulting in background gradients. The problems resulting directly from the gradient pulses themselves are discussed in the next section.

In the absence of gradient pulses, there should be zero current flowing through the gradient coils; however, in practice slight differences in potential difference between different parts of the spectrometer (e.g., the amplifier and the input line may not have the same zero voltage) cause currents to flow through the gradient coils between pulses, resulting in nonrandom gradients. Similarly, the amplifier will also have a noise level resulting in small currents through the coils. Although very small, such earth loop and noise currents result in troublesome background gradients and can completely thwart high-resolution diffusion experiments, since they will be present during signal acquisition (similar to bad shimming) as well as attenuating the signal as in the normal Hahn spin-echo sequence (see Part 1, Eq. [17]). Ideally, one would have an oscilloscope available when tracing noise problems on a spectrometer, but the observed spectrum itself forms an extremely sensitive probe. Earth loop currents can be detected by physically disconnecting the gradient circuit and looking at the effect on the line shape or shift of the signal in the observed spectrum, or, if available, by the effects on the lock signal. The effects of amplifier noise can be further assessed by observing a spectrum with and without the amplifier turned on (n.b., with the inputs of the amplifier shorted).

To prevent the effects of earth loops and noise, all of the components in the spectrometer and current amplifier should be earthed to the same point, and ideally, the gradient coil should be blanked (i.e., disconnected) from the current circuit between gradient pulses (Fig. 2). Blanking, however, will not prevent the effects of noise during the gradient pulses. Very small earth loop effects can be shimmed out if the earth loop currents result in a steady gradient.

Although the pulse program clearly defines when the spectrometer should send logic or shaped voltage pulses to the current amplifier, the logic line or shaped voltage line from the spectrometer to the amplifier may not be delivering clean pulses to the amplifier, and some degree of noise is common. This noise will, of course, be amplified by the amplifier resulting in gradient noise (i.e., randomly changing gradients). This noise problem is compounded by the amplifier's inherent noise level. The input noise can be detected by observing a spectrum before and after shorting the input to the gradient amplifier (n.b., the gradients are not pulsed) and looking at the effect on the line shape or shift of the signal in the observed spectrum, or, if available, by the effects on the lock signal.

Stable and perfectly reproducible gradient pulses are crucial for accurate PFG measurements. In a modern spectrometer, accurate timing of pulses and their duration is generally not a problem. The major sources of imprecision are, as noted above, the noise in the gradient system, and it may not necessarily be uniform with time and the instability of the amplifier. However, it has also been noted that the refocusing rf pulse (i.e., the π pulse in the Stejskal and Tanner sequence) induces a signal in the gradient coils, which in turn elicits a small current pulse from the current amplifier (*26*) (although this problem can be overcome by a more sophisticated gradient driver design). As we will discuss in detail below, the defocusing and refocusing effects of the gradient pulses in the pulse sequence must be very finely matched. We note that the gradient magnitude needed to measure a dynamic displacement n orders of magnitude smaller than the sample dimensions will result in a dephasing of order 10^n cycles across the sample and that the refocusing must be accurate to within a few degrees (see Fig. 2 of Part 1). Thus, for example, to measure a displacement of 0.1 μm in a 5-mm tube, the gradient pulse pair must be matched to better than 1 in 10^5 (*2*); thus, the greater the stability and the lower the noise of the system, the better. We also note that the gradient pulses themselves contribute to the problem themselves owing to the generation of eddy currents; this will be discussed in detail in the next section. The—in some ways—related effect of sample movement was considered in Sample Movement with Respect to the Gradient. As mentioned in Amplifiers, the effects of gradient coil heating are normally overcome by the use of a constant current amplifier. However, it may be that the amplifier is incapable of producing two equally matched gradient pulses in quick succession. A means of increasing the reproducibility of the pulses is to place additional, appropriately spaced (i.e., Δ apart) gradient pulses

prior to the start of the rf pulse sequence [see Fig. 8(B)].

To illustrate the effects of imperfectly matched gradient pulses, we consider the Stejskal and Tanner pulse sequence. We recall from Part 1 that for a single nondiffusing spin at position z, and considering only the effects of the applied gradient pulses (we denote g as $g(t)$ to emphasize the time dependence of the gradient pulse), the cumulative phase shift at 2τ is given by

$$\phi(2\tau) = \gamma\left[\int_0^{\tau} g(t')z\,dt' - \int_{\tau}^{2\tau} g(t')z\,dt'\right] \quad [6]$$

and that the normalized intensity (i.e., an attenuation) of the echo signal at 2τ is given by (*27*, *28*) (see Part 1, Eqs. [10–12]),

$$S(2\tau) = S(2\tau)_{g=0}\int_{-\infty}^{\infty} P(\phi, 2\tau)\cos\phi\,d\phi \quad [7]$$

where $S(2\tau)_{g=0}$ is the signal (i.e., resultant magnetic moment) in the absence of a field gradient and $P(\phi, 2\tau)$ is the (relative) phase-distribution function which for the case of a single spin is equal to unity. From Eq. [7], we can see that if $\phi = 0$, the echo will be maximum and properly phased. Thus, only if the gradient pulses are perfectly matched [i.e., the integral over the gradient in the first τ period matches that in the second τ period (Eq. [6])] will the echo maximum occur at $t = 2\tau$. If they do not, and acquisition is begun at $t = 2\tau$, the echo will not be in phase and its intensity will be reduced. If the degree of mismatch fluctuates, the position of the echo maximum will also fluctuate. In the case of an ensemble of spins at different positions, z, the magnetization helix (*29*) will not be properly unwound (i.e., there will be a residual phase twist; consider the top series of spin phase diagrams in Fig. 2 of Part 1). Writing in terms of q, the phase twist resulting from a gradient pulse mismatch of $\Delta\mathbf{q}$ (here, Δ denotes differential, not the delay in the pulse sequence) would be given by

$$\phi_{\text{phase twist}} = \exp(i2\pi\Delta\mathbf{q}\cdot\mathbf{r}) \quad [8]$$

In the observed spectrum, the phase problem would not be evident and the observed signal intensity will be severely reduced, since the vector sum of the magnetization helix in the x–y plane will be close to zero. Out of simplicity, we have taken $g(t)$ to reflect only the applied gradient pulses; in reality, $g(t)$ in Eq. [6] contains all gradients present (i.e., noise gradients, B_0 imperfection, and internal gradients). The effects of internal gradients will be considered in Short Relaxation Times, Internal Gradients, and Other Problems.

The equation describing the echo attenuation for the Stejskal and Tanner sequence where the second gradient pulse is mismatched by a duration ε longer than the first pulse (Table 1) can be readily derived using the theory presented in the first article (see Part 1, The Macroscopic Approach) and is found to be (*30*)

$$E = \exp(-\gamma^2 g^2 D\{\delta^2(\Delta - \delta/3) + \varepsilon^2(2\tau - t_1 - \Delta - \delta - 2\varepsilon/3)\}) \quad [9]$$

It can be seen that the mismatch introduces a τ and t_1 dependence to the equation; interestingly, though, ε enters into the equation in second order (*31*). However, whereas the mismatch may have only a small effect on the attenuation due to the diffusion, the signal may be unobservably small.

One solution to mismatched gradient pulses is to finely adjust the magnitude or (more easily) the duration of one of the gradient pulses with respect to the other (see, for example, Fig. 2 in Ref. *32*). For example, the Stejskal and Tanner sequence could first be performed in the absence of gradient pulses and used to determine the reference phase setting. Subsequently, the same experiment could be performed but using gradient pulses. If the gradient pulses are perfectly matched, a maximum echo will occur at $t = 2\tau$. However, this is an empirical approach and is dependent on the experimental times and gradient strengths used, and may not even be applica-

Table 1 g(t) for the Stejskal and Tanner Sequence with Mismatched Gradient Pulses

Subinterval of Pulse Sequence	$\mathbf{g}(t)$
$0 < t \le t_1$	0
$t_1 < t \le t_1 + \delta$	g
$t_1 + \delta < t \le t_1 + \Delta$	0
$t_1 + \Delta < t \le t_1 + \Delta + \delta$	g
$t_1 + \Delta + \delta < t \le t_1 + \Delta + \delta + \varepsilon$	g
$t_1 + \Delta + \delta + \varepsilon < t \le 2\tau$	0

ε represents the degree of mismatch of the second gradient pulse. If $\varepsilon = 0$, then the sequence corresponds to that given in Fig. 1.

ble if the source of the mismatch is due to eddy current–generated gradients that are not parallel to the applied gradients (*33*) or nonconstant mismatch. We also note that the MASSEY sequence can be used to alleviate the phase-twist problem (see Postprocessing). The phase-twist problem is considered in more detail in that section.

Eddy Currents and Perturbation of B_0

The rapid rise of the gradient pulses can generate eddy currents in the surrounding conducting surfaces around the gradient coils (e.g., probe housing, cryostat, radiation shields, etc.). The severity of the eddy current problem is thus proportional to dI/dt and the strength of the gradient. Although the generation of eddy currents is greatly decreased through the use of shielded gradient coils (see Gradient Coils), they can still occur, especially when using large, rapidly rising and falling gradient pulses. The eddy currents, in turn, generate additional magnetic fields and thus have a close relationship to the problems discussed in the previous section. It is the decay of the eddy currents and their associated magnetic fields that determine the minimum delay that must be left between the end of the gradient pulse and the start of spectral acquisition. Eddy currents can have the following effects: (a) phase changes in the observed spectrum and anomalous changes in the attenuation, (b) gradient-induced broadening of the observed spectrum, and (c) time-dependent but spatially invariant B_0 shift effects (which appears as ringing in the spectrum).

We illustrate the effects of eddy currents using the Stejskal and Tanner sequence as an example. If the eddy current tail from the first gradient pulse extends into the second τ-period, then the total field gradient during the second evolution period will not equal that in the first and the situation is analogous to the case of mismatched pulses [see Amplifier Noise, Earth Loops, and Nonreproducible (Mismatched) Gradient Pulses]. Consequently, even if a spin has not moved in the direction of the gradient during the sequence, there will be a residual phase shift. As a result, the point at which the maximum echo appears will be shifted and its amplitude will be affected (*34*). Thus, assuming that signal acquisition is begun as usual, at $t = 2\tau$ the eddy currents will cause additional attenuation unrelated to diffusion, and perhaps if the eddy currents have not dissipated before acquisition begins, phase shifts and spectral broadening.

To gain some insight into the effects on the echo attenuation if the eddy currents generated by the first gradient pulse have not dissipated before the application of the π pulse, and similarly, if the disturbances generated by the second gradient pulse have not dissipated prior to the start of acquisition, assuming infinitely fast rise and but exponential fall (with exponential rate constant k) of the gradient pulses (Table 2), we can derive the echo attenuation equation for the Stejskal and Tanner sequence using the same method as before (see Part 1, The Macroscopic Approach). An example program using the symbolic algebra package Maple (*35*) is given in the Appendix (n.b., the new definition of the function `F` to allow for time-dependent gradients). The attenuation equation is given by

$$E = \exp(-\gamma^2 g^2 D\{\delta^2(\Delta - \delta/3) + f(t)\}) \quad [10]$$

Table 2 $\mathbf{g}(t)$ for the Stejskal and Tanner Sequence in Which Eddy Currents Generated by the First Gradient Pulse Have Not Totally Decayed by the Time of Application of the π Pulse (A Similar Situation is Depicted in Fig. 5, if t_e Is Shorter Than the Time Required for the Eddy Current Effects to Dissipate) and Similarly the Eddy Currents from the Second Gradient Pulse Extending into the Acquisition Period

Subinterval of Pulse Sequence	$\mathbf{g}(t)$
$0 < t \le t_1$	0
$t_1 < t \le t_1 + \delta$	g
$t_1 + \delta < t \le t_1 + \Delta$	$ge^{-k(t-t_1-\delta)}$
$t_1 + \Delta < t \le t_1 + \Delta + \delta$	g
$t_1 + \Delta + \delta < t \le 2\tau$	$ge^{-k(t-t_1-\Delta-\delta)}$

k is the exponential rate constant.

where

$$
\begin{aligned}
f(t) = \frac{1}{k}\Bigg(& 2\delta\Delta - \delta^2 + \delta^2 e^{-k(\Delta-\delta)} \\
& + 4\delta e^{-k(\tau - t_1 - \delta)}\left[\tau - \Delta - t_1 - \frac{\delta}{2}\right]\Bigg) \\
& + \frac{1}{k^2}\big(\Delta - 2\delta + 4\tau e^{-2k(\tau - t_1 - \delta)} \\
& + 4[\tau - \Delta - t_1]e^{-k(\tau - t_1 - \delta)} \\
& + [2\tau - \Delta - t_1] \\
& \quad \times (e^{-2k(\Delta-\delta)} - 4e^{-k(\Delta + \tau - t_1 - 2\delta)})\big) \\
& + \frac{1}{2k^3}(8e^{-k(\tau + \Delta - t_1 - 2\delta)} \\
& + 8e^{-k(3\tau - \Delta - 2t_1 - 2\delta)} - 4e^{-k(2\tau - t_1 - 2\delta)} \\
& - 8e^{-2k(\tau - t_1 - \delta)} - e^{-2k(\Delta - \delta)} \\
& - e^{-2k(2\tau - \Delta - t_1 - \delta)} - 1)
\end{aligned}
$$

This analysis is simplistic in the expression of the form of the eddy currents and also because it does not consider the effects of the phase twist on the observed signal.

Except for some cases of restricted diffusion (*36*), a plot of $\ln(E)$ versus $\gamma^2 g^2 \delta^2(\Delta - \delta/3)$ is normally linear in the case of free diffusion, or upward concave in the case of more complicated systems; von Meerwall and Kamat (*33*) remarked that downward curvature is indicative of eddy current effects. Convection can also result in downward curvature.

To determine if eddy current effects are significant, a measurement can be performed on a sample such as an extremely large monodisperse polymer with a diffusion coefficient lower than that which can be detected with the experimental system and parameters (i.e., δ, Δ, and **g**) in question (see Gradient Calibration). If the signal is attenuated or distorted, then the presence of eddy current effects is implied. Another simple way to determine if eddy current effects are present, and in particular to determine the minimum settling delay, t_e, needed is to use the pulse sequence shown in Fig. 5 (*34*). Some example spectra acquired using this pulse sequence are shown in Fig. 6. Eddy current fields can also be measured using search coils (*17*), but such techniques are beyond the scope of the present article and are more commonly used in large imaging systems.

Especially in the case of large gradients, the rapid rise and fall of the pulses can directly affect the stability of the main magnetic field by inducing additional currents into the solenoids producing the main magnetic field, or indirectly by affecting the lock feedback system. The final result is that the main field may be caused to oscillate or at least shift from its normal value (i.e., a time-dependent but spatially invariant B_0 shift) (*37*). In such a case, if the ringing persists through acquisition, the observed spectrum will appear to be something like a spectrum observed with a continuous-wave NMR spectrometer.

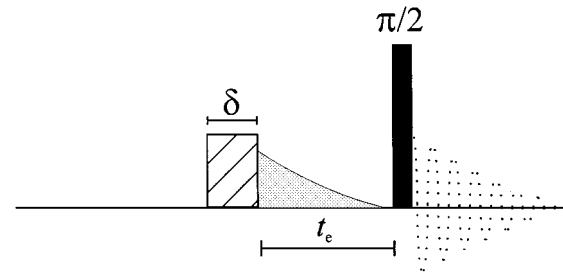

Figure 5 A simple pulse sequence to determine the minimum time necessary for the effects of eddy currents to dissipate. In this sequence, a gradient pulse is first applied. After a delay t_e, an rf pulse (not necessarily $\pi/2$) is applied and a spectrum is acquired. Spectra are acquired with successively shorter t_e delays to determine the minimum time required for the eddy current effects to decay. Some examples of experimental spectra are shown in Fig. 6.

As noted above, shielded gradient coils may not sufficiently reduce the eddy currents generated in the surrounding conducting metals (n.b., they could still be generated in the rf coil—if their design allows circulating low-frequency currents). Eddy current problems are especially problematic when dealing with species with short T_2 relaxation times, where it is impossible to sufficiently increase the delay after the gradient pulse to allow the eddy current effects to subside. Thus, we now consider further approaches for minimizing or coping with the effects of eddy currents. We can roughly divide the approaches into two categories: (a) hardware solutions, and (b) pulse sequence and postprocessing.

Hardware Solutions. Several methods exist for handling the eddy current problems. The most effective solution, as noted above, is to use shielded gradient coils (see Gradient Coils). This method is particularly convenient since no experimental adjustments are necessary. Another commonly used approach is termed "pre-emphasis." The method is based on the Lenz's law requirement that the sign of the fields generated by the eddy currents will be opposed to the change which

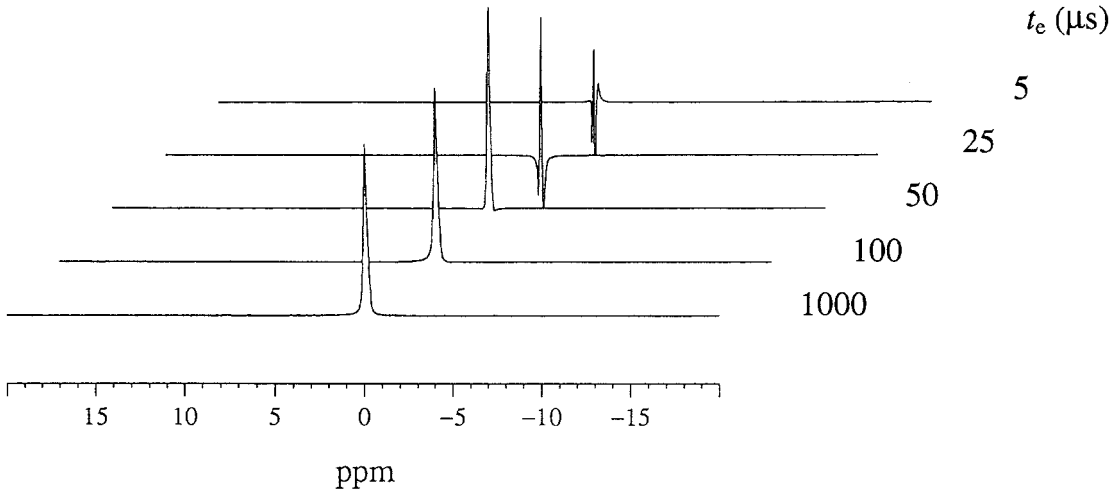

Figure 6 Experimental spectra acquired using a sample of $^{13}CCl_4$ and the pulse sequence given in Fig. 5 for various values of t_e. The gradient pulse used had a duration of 1 ms and a strength of 0.45 T m^{-1}. Eddy current effects result in the spectra appearing to be badly phased. From these spectra, it can be seen that (using these gradient parameters) a delay $\geq$ 100 μs should be set to allow for the eddy current effects to decay.

induced them. Thus, the current at the leading and tailing edges of the gradient pulses is overdriven, and in this way the coils self-compensate for the induced eddy currents. This is generally performed by adding numerous small exponential corrections of different amplitude and time constants to the desired current waveform (*37–39*). Pre-emphasis is depicted in Fig. 7. In performing pre-emphasis, the difference between the desired and the measured gradient waveform indicates the distortion due to the eddy currents. Typically, pre-emphasis uses three time constants and is performed in the software, in which case an appropriately shaped voltage waveform is sent to the amplifier, although it is possible with additional circuitry to add pre-emphasis to a rectangular logic pulse generated before reaching the amplifier. The pre-emphasis time constants are then determined using an iterative approach with the sequence shown in Fig. 5 to adjust the various time constants. In practice, pre-emphasis is experimentally complicated and the method is not perfect, since the spatial distribution of the fields produced by the eddy currents in the surrounding metal and those produced by the gradient coils are not identical (*40*). Nevertheless, pre-emphasis is commonly used even with shielded coil systems to improve performance.

Another hardware approach is aimed at stabilizing the field homogeneity after a gradient pulse by dynamic shimming and B_0 compensation (e.g., pulsing a B_0 coil simultaneously to the gradient pulse) (*39*, *41*, *42*). For example, some commercially available PFG probes contain a set of z and z^2 shims which are pulsed in unison with the gradient coil.

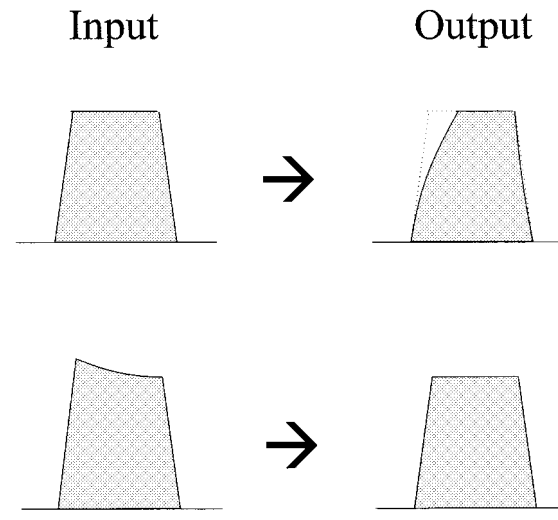

Figure 7 A conceptual idea of the pre-emphasis procedure. Ideally, the input waveform (i.e., current pulse) (top left) into the gradient coil would produce a gradient pulse of the same shape. However, owing to the generation of eddy currents, the resulting gradient waveform is distorted (top right) (the desired gradient shape is denoted by dots). A solution is to shape the input waveform to counteract the eddy current effects (bottom left) and thereby produce the desired gradient shape.

Pulse Sequences and Postprocessing Solutions.

Introduction. For most users, modification to the hardware is not a practical solution and the use of pulse sequences to minimize the effects of eddy currents on the diffusion measurements will be the only recourse. Pulse sequence solutions involve delaying the acquisition until the eddy currents have dissipated; avoiding the generation of eddy currents; compensating for their effects; or, in combination with postprocessing, correcting for their effects. We should also mention that multiple quantum experiments (see Multiple Quantum and Heteronuclear Experiments) can be used to reduce the gradient magnitudes required, and thus the size of the eddy currents; however, these sequences are applicable only to some samples, specifically those in which it is possible to generate multiple quantum transitions. It should be noted that although smaller eddy currents are generated owing to the decreased gradient requirements in multiple quantum experiments, multiple quantum experiments will be more sensitive to the presence of eddy currents.

Adjusting the Duration of Individual Gradient Pulses. As noted in Amplifier Noise, Earth Loops, and Nonreproducible (Mismatched) Gradient Pulses, eddy currents can have the effect of making the gradient pulses mismatched (*31–34*), and the same solutions apply as outlined for imperfect pulses (see the same earlier section). However, the intentional mismatching of pulses is not an optimal procedure for overcoming eddy current distortions, since the correction will depend on the particular experimental parameters, and thus, the correction factor will not be general. Further, the eddy current–generated fields may not be even in the same direction as the applied gradients, and thus mismatching may offer no solution (*33*).

Delaying the Acquisition until the Eddy Currents Have Dissipated. Another commonly used pulse sequence approach which requires no special hardware is to delay the acquisition until the effects of the eddy currents have dissipated. Many such sequences are based on the stimulated echo sequence (STE) [Fig. 8(A)]. The STE pulse sequence has one extremely important difference from the standard PFG pulse sequence in that the major part of the duration Δ can be contained in the τ_2 period, where the magnetization is aligned along the z axis, where it is subject only to T_1 relaxation. This is particularly important since for many species, especially macromolecules, $T_1 \gg T_2$, and thus, Δ can be of sufficient length while allowing τ_1 to be long enough to let the eddy current effects dissipate. Griffiths et al. (*43*) proposed an experiment in which a train of π rf pulses is used to refocus the stimulated echo so as to delay the acquisition until after the eddy currents have subsided. However, since the magnetization is transverse during this period, it is susceptible to transverse relaxation,

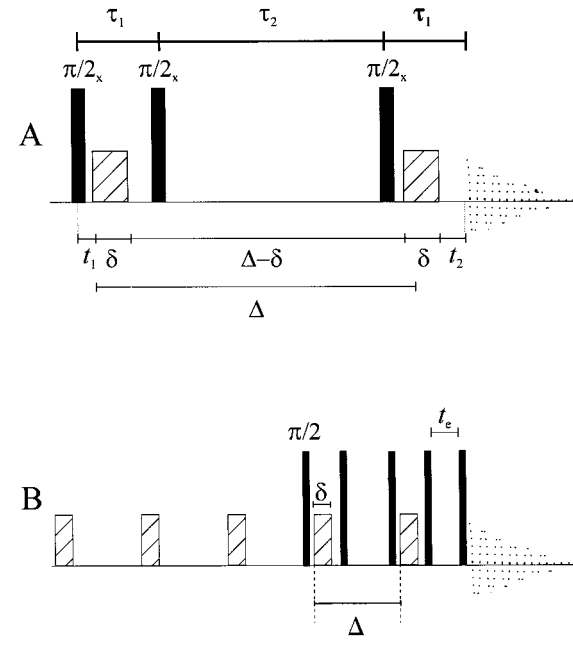

Figure 8 (A) The stimulated echo (STE) pulse sequence (*45*, *47*). A notable feature of the STE sequence is that for most of Δ (specifically during the period τ_2), the magnetization is aligned along the z axis and is subject only to longitudinal relaxation; however, during the first and last period (i.e., the two τ_1 delays), the magnetization is transverse and is subject to spin–spin relaxation. Since for macromolecules $T_1 > T_2$, the STE sequence is generally preferred to the Stejskal and Tanner sequence (see Fig. 15) and it is preferable to keep $\tau_1 \ll \tau_2$. It should be noted that the naming convention follows that of van Dusschoten et al. (*86*) and not the more commonly used scheme of Tanner (*45*) (i.e., Tanner's τ_2 is defined as the duration between the first and third $\pi/2$ pulses, which is equal to $\tau_1 + \tau_2$ in the present work), consequently, the definition of Eqs. [33] and [36] appears different (although equivalent) from that found in some references [e.g., (*45*)]. (B) The longitudinal eddy current delay (LED) pulse sequence (*44*). The eddy current disturbances are able to decay during the delay t_e before signal acquisition. A series of gradient prepulses are shown separated by Δ.

J modulation (see J Modulation) and phase distortions from the eddy currents. A commonly used approach is the longitudinal eddy current delay (LED) pulse sequence [Fig. 8(B)] (*44*). This is a modified STE experiment and is useful when the T_1's of the species in question are longer than the lifetime of the eddy current transients. However, the LED sequence does not solve the problem of the eddy current tail extending from the first gradient pulse into the second transverse evolution period. A partial solution is to precede the sequence by a train of identical gradient pulses with the same separation as that used in the LED sequence (*31*, *33*). A problem common to both the STE and LED sequences is that as many as five echoes (four spin-echoes as well as the stimulated echo) result, and extensive phase cycling must be used to remove the effects of the other echoes (*45–47*). The phase-cycling requirements of both sequences can be greatly reduced if a homospoil pulse is included after the second rf pulse.

Bipolar Gradients. A more elegant solution than waiting for the effects of the eddy currents to dissipate, although requiring more sophisticated gradient control, is the use of self-compensating (or bipolar) gradient pulses (*46*, *48*) (Fig. 9). In this method, a gradient pulse of duration δ is replaced by two gradient pulses of duration $\delta/2$ with a π rf pulse in between the two gradient pulses. The two gradient pulses are of opposite sign and the π rf pulse has the effect of negating the phase change induced by the first pulse such that taken as a whole, this bipolar-gradient-rf-pulse sandwich is equivalent to a gradient pulse

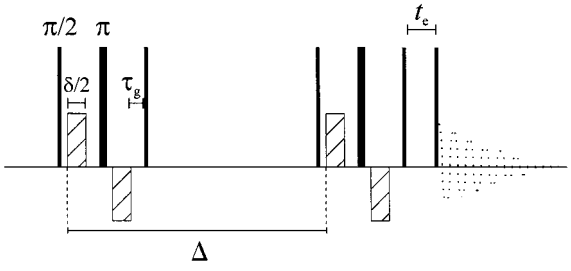

Figure 9 An LED pulse sequence incorporating bipolar gradient pulses. The phase cycling for the different pulses is given in Ref. *46*. The self-compensating effects of the bipolar gradient pulse sandwiches largely cancel the generation of eddy currents. The two π pulses in the bipolar-gradient pulse sandwiches have the beneficial effect of reducing the active volume of the sample to the region of homogeneous rf.

of duration δ with the polarity of the second gradient pulse in the sandwich. Since eddy currents typically have settling times of the order of hundreds of milliseconds, the eddy currents generated by the first pulse of, for example, positive polarity are canceled by the effects of the second gradient (negative) pulse in the sandwich which follows at most only a few milliseconds later. An example of using bipolar gradient pulses in an LED sequence is given in Fig. 9. Similar to the simple Stejskal and Tanner sequence, the signal attenuation due to diffusion is related by the following equation (the time periods are defined in Fig. 9) (*46*)

$$E = \exp\left(-\gamma^2 D g^2 \delta^2 (\Delta - \delta/3 - \tau_g/2)\right) \quad [11]$$

Modulated Gradients. Nearly all PFG sequences prescribe rectangular gradient pulses. However, the usage of rectangular pulses lies more in mathematical simplicity than from a physical requirement. As noted above the severity of the eddy currents is proportional to dI/dt; hence, an obvious means of reducing eddy current effects is to slow the rise and fall times of the gradient pulses. With many modern spectrometers having the ability to generate shaped pulses, sine and trapezoidal gradient pulses are commonly used. Here, we examine the effect of such pulses in the standard Stejskal and Tanner PFG pulse sequence in the absence of background gradients. For the case of rectangular or nearly rectangular gradient pulses [Figure 10(A) and Table 3], the solutions can be determined by using the theory developed in the first article (see Part 1, The Macroscopic Approach) and are found to be of the form (*30*)

$$E = \exp(-\gamma^2 g^2 D\{\delta^2(\Delta - \delta/3) + f(t)\}) \quad [12]$$

where the $f(t)$ term is defined later in Table 5. By substituting reasonable values for the gradient pulse parameters, it is easy to show (*30*) that if the pulses are nearly rectangular, the precise shape is unimportant as long as the area (i.e., δg) of each pulse is equal to that of the ideal rectangular pulse. In the case of sine or sine^2 gradient pulses [Fig. 10(B) and Table 4], the following relations can be derived (*30*):

$$E_{\sin} = \exp\left(-\gamma^2 g^2 D\delta^2\left[\cos^2\left(\frac{N\pi}{2}\right)3\delta + \sin^2\left(\frac{N\pi}{2}\right)(4\Delta - \delta)\right]\Big/(N\pi)^2\right) \quad [13]$$

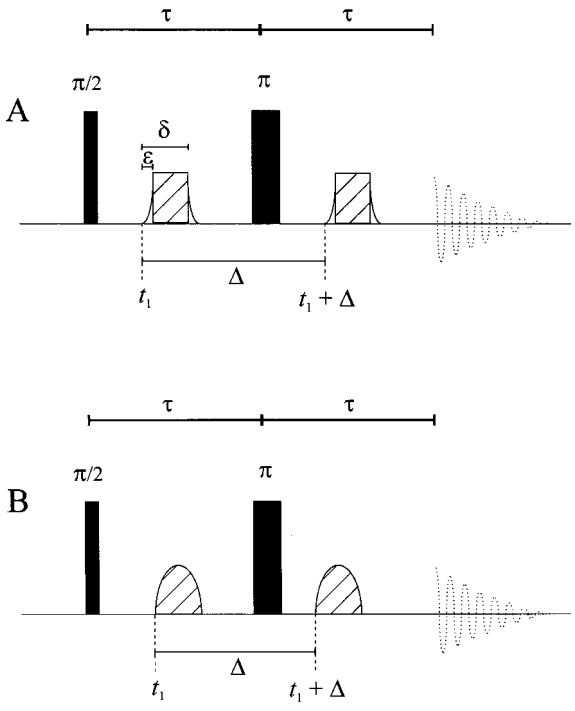

Figure 10 Example of the Stejskal and Tanner pulse sequence incorporating shaped gradient pulses (A) nearly rectangular and (B) sinusoidal. Since the generation of eddy currents is proportional to dI/dt, the use of shaped gradient pulses is a convenient means of reducing eddy current generation. However, it is mathematically more difficult to relate their effects to the attenuation of the echo signal.

$$E_{\sin^2} = \exp\left(-\gamma^2 g^2 D\delta^2\left(\Delta/4 + \delta/12 + 5\delta/(4N\pi)^2\right)\right) \quad [14]$$

where $2N$ (N is an integer) denotes the period of the gradient pulse.

For completeness, we note that some other gradient shapes have been studied in the literature (*49–51*). We need to stress, however, that sequences containing such shaped gradient pulses are only possible on sophisticated spectrometers capable of generating shaped waveforms.

Postprocessing. The basic idea of postprocessing, instead of preventing the eddy current effect, is to correct the measured FID for the eddy current effects. Thus, postprocessing does not reduce the eddy current distortions of the gradient pulses themselves, but it does reduce distortion in the acquired spectra. The simplest postprocessing scheme is to measure the phase of an on-resonance signal from a single component spectrum as it evolves following a gradient pulse. This

Table 3 $\mathbf{g}(t)$ for the Stejskal and Tanner Sequence for Ramped and Exponentially Shaped Gradient Pulses [see Fig. 10(A)]

Subinterval of Pulse Sequence	Ramped Rise and Fall of $\mathbf{g}(t)$	Exponential Rise and Fall of $\mathbf{g}(t)$	Exponential Rise and Fall with Overshoot and Undershoot of $\mathbf{g}(t)$	Sine Rise and Fall of $\mathbf{g}(t)$
$0 < t \le t_1$	0	0	0	0
$t_1 < t \le t_1 + \varepsilon$	$(g/\varepsilon)(t - t_1)$	$g(1 - e^{-k(t-t_1)})$	$g + k(t - t_1)e^{-k(t-t_1)}$	$g \sin((t - t_1)\pi/(2\varepsilon))$
$t_1 + \varepsilon < t \le t_1 + \delta$	g	g	g	g
$t_1 + \delta < t \le t_1 + \delta + \varepsilon$	$g[1 - (1/\varepsilon)(t - t_1 - \delta)]$	$ge^{-k(t-t_1-\delta)}$	$-k(t - t_1 - \delta)e^{-k(t-t_1-\delta)}$	$g[1 - sin((t - t_1 - \delta)\pi/(2\varepsilon))]$
$t_1 + \delta + \varepsilon < t \le t_1 + \Delta$	0	0	0	0
$t_1 + \Delta < t \le t_1 + \Delta + \varepsilon$	$(g/\varepsilon)(t - t_1 - \Delta)$	$g(1 - e^{-k(t-t_1-\Delta)})$	$g + k(t - t_1 - \Delta)e^{-k(t-t_1-\Delta)}$	$g \sin((t - t_1 - \Delta)\pi/(2\varepsilon))$
$t_1 + \Delta + \varepsilon < t \le t_1 + \Delta + \delta$	g	g	g	g
$t_1 + \Delta + \delta < t \le t_1 + \Delta + \delta + \varepsilon$	$g[1 - (1/\varepsilon)(t - t_1 - \delta - \Delta)]$	$ge^{-k(t-t_1-\Delta-\delta)}$	$-k(t - t_1 - \Delta - \delta)e^{-k(t-t_1-\Delta-\delta)}$	$g[1 - sin((t - t_1 - \Delta - \delta)\pi/(2\varepsilon))]$
$t_1 + \Delta + \delta + \varepsilon < t \le 2\tau$	0	0	0	0

k is the rate constant that describes the exponential rise and fall of the gradient pulse. The corresponding echo attenuation equations are given by Eq. [12] and Table 5.

Table 4 $g(t)$ for the Stejskal and Tanner Sequence for Sinusoidally Shaped Gradient Pulses [see Fig. 10(B)]

Subinterval of Pulse Sequence	Sine-shaped $\mathbf{g}(t)$	Sine^2-shaped $\mathbf{g}(t)$
$0 < t \leq t_1$	0	0
$t_1 < t \leq t_1 + \delta$	$g \sin(N(t - t_1)\pi/\delta)$	$g \sin(N(t - t_1)\pi/\delta)^2$
$t_1 + \delta < t \leq t_1 + \Delta$	0	0
$t_1 + \Delta < t \leq t_1 + \Delta + \delta$	$g \sin(N(t - t_1 - \Delta)\pi/\delta)$	$g \sin(N(t - t_1 - \Delta)\pi/\delta)^2$
$t_1 + \Delta + \delta < t \leq 2\tau$	0	0

$2N$ (N is an integer) denotes the period of the gradient pulse. The corresponding echo attenuation equations are given by Eqs. [13] and [14].

reference phase-angle evolution can then be subtracted from all subsequent spectra obtained under the same conditions to remove the effect of B_0 variation (*52*). Other variations based on deconvolution using an experimental reference exist (*53*).

In work related to the helix picture of magnetization subjected to a constant gradient (*29*), Callaghan developed the MASSEY sequence (*21*) for minimizing phase instability in very-high-gradient NMR spectroscopy (Fig. 11). The method also corrects for sample movement (see Sample Movement with Respect to the Gradient). This method incorporates a read gradient (i.e., k space; this usage of k is not to be confused with the exponential rate constant used above), G, into the standard Stejskal and Tanner sequence; thus, in a sense, it is also a pulse sequence solution and not only a postprocessing solution. It is important to realize that in this method the same gradient coil is used for generating the gradient pulses and also the read gradient. The addition of G allows for the restoration of spatially dependent phase shifts such as those caused by a mismatch in the (q-space) gradient pulses. To understand how this method works, we need to consider the mathematics behind the phase-twist problem. We start from the average propagator representation of the short gradient pulse approximation (see Eq. [87], Part 1), except we now include the effects of a phase shift, ϕ, due to the effects of a gradient mismatch [see Amplifier Noise, Earth Loops, and Nonreproducible (Mismatched) Gradient Pulses], $\Delta\mathbf{q}$, and of movement $\Delta\mathbf{r}_o$ of the entire (i.e., rigid) sample (see Sample Movement with Respect to the Gradient) between the first and second gradient pulses in the Stejskal and Tanner sequence. Thus, we have

$$E(\mathbf{q}, \Delta) = \int \bar{P}(\mathbf{R}, \Delta) e^{i[2\pi\mathbf{q}\cdot\mathbf{R} + \phi]}\, d\mathbf{R} \qquad [15]$$

where $\bar{P}(\mathbf{R}, \Delta)$ is the average propagator and $\mathbf{R}$ is the dynamic displacement defined by $\mathbf{r}_1 - \mathbf{r}_0$ (the starting and finishing positions of a spin with respect to the first and second gradient pulses) and

$$2\pi\mathbf{q}\cdot\mathbf{R} + \phi = 2\pi[(\mathbf{q} + \Delta\mathbf{q})\cdot(\mathbf{r}_0 + \mathbf{R} + \Delta\mathbf{r}_o) - \mathbf{q}\cdot\mathbf{r}_o]. \qquad [16]$$

Table 5 The $f(t)$ Term in Eq. [12] for the various B_0 gradient pulse shapes in the Stejskal and Tanner Sequence (see Fig. 10) given in Table 3

Gradient Pulse Shape	$f(t)$
Ramped rise and fall	$\varepsilon^3/30 - \delta\varepsilon^2/6$
Exponential rise and fall	$-2/k^2(1/k - \delta) + 4/(ke^{\varepsilon k})(\varepsilon\delta - 1/k^2 - \varepsilon^2/2)$ $+2/(k^2e^{2\varepsilon k}) \times (\delta + 1/k)$
Exponential rise and fall with overshoot and undershoot	$(-8\delta/k^2 - 12/k^3 + e^{-\varepsilon k}(2\varepsilon^2 - 4\varepsilon^2\delta + 6\varepsilon^2/k$ $-8\delta\varepsilon/k + 12\varepsilon/k^2 - 8\delta/k^2 + 12/k^3))/g$ $+4e^{-\varepsilon k}(\varepsilon^2 - \varepsilon\delta - \delta/k)/(g^2k) + e^{-2\varepsilon k}(2\varepsilon^2\delta + 6\varepsilon^2/k$ $+4\varepsilon\delta/k + 6\varepsilon/k^2 + 2\delta/k^2 + 3/k^3)/g^2$ $+(2\delta - 3/k)/(g^2k^2)$
Sine rise and fall	$4\varepsilon^2(\varepsilon - 2\delta)/\pi + 8\varepsilon^2(\varepsilon - 3\delta)/\pi^2 - 64\varepsilon^3/\pi^3$

From Price and Kuchel (*30*).

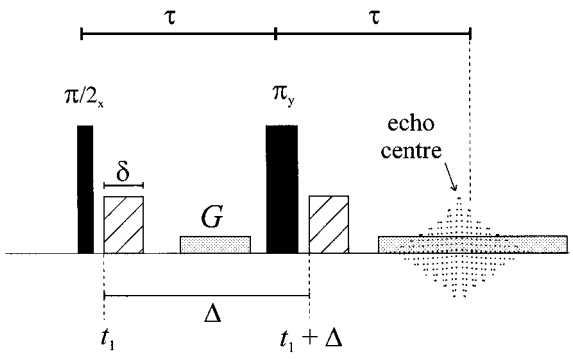

Figure 11 The sequence used in the MASSEY technique for removing phase instability (*21*). The sequence is a combination of the Stejskal and Tanner sequence with a read gradient, G.

Since we take $\mathbf{q}$ to be oriented along the z direction, we are concerned only with the z component of $\Delta\mathbf{r}_o$, Δz_o. Furthermore, we assume that $\Delta\mathbf{q}$ is parallel to $\mathbf{q}$ (i.e., a magnitude mismatch), and so Eq. [16] becomes

$$2\pi\mathbf{q}\cdot\mathbf{R} + \phi = 2\pi[qZ + (q + \Delta q)\Delta z_o + \Delta q z_o] \quad [17]$$

and thus, Eq. [15] can be rewritten

$$E(q,\Delta) = \underbrace{\int \bar{P}(Z,\Delta)e^{i2\pi qZ}\,dZ}_{E_0(q,\Delta)} \underbrace{e^{i2\pi(q+\Delta q)\Delta z_o}}_{\text{sample motion}} \times \underbrace{\int \rho(z_0)e^{i2\pi\Delta q z_o}\,dz_0}_{\mathbf{z}\text{-dependent phase twist}} \quad [18]$$

where $\rho(z_0)$ is the spin density. The first term in Eq. [18] (i.e., $E_0(q,\Delta)$) is the ideal case, i.e., the attenuation due to diffusion, and it is what we really want to measure. The second term is the net phase shift that results from sample motion. The third term results from the gradient pulse mismatch and is the integral of the position-dependent phase shifts (this has clear similarity to **k**-space encoding in imaging, e.g., Refs. *2*, *8*, *54*) and can be removed only after the spatial dependence is known—hence the inclusion of the read gradient into the pulse sequence. It is the third term that can result in severe artifactual signal attenuation.

We now need to consider the requirements for spatially separating the phase shifts using the imaging process with the read gradient. Suppose that N points in the k-space dimension are sampled with a sampling interval of T. The spectral separation of adjacent pixels in k space will then be $1/NT$, which corresponds to a spatial separation of $2\pi/(\gamma GNT)$. Thus, we require that this be less than or equal to the wavelength of the phase twist so that the phase modulation is well resolved. Thus, we require

$$\frac{2\pi}{\gamma GNT} > \frac{1}{\Delta q} \Rightarrow G > \frac{2\pi\Delta q}{\gamma NT} \quad [19]$$

It is desirable to keep the acquisition time as long as possible providing that the pixel separation is larger than the homogeneous linewidth ($\nu_{1/2} = \pi T_2$), which sets the lower bandwidth limit as

$$\frac{1}{T} \geq \frac{N}{\pi T_2} \quad [20]$$

The phase twist caused by pulse mismatch is resolved by Fourier transformation of the whole echo with respect to k ($= (2\pi)^{-1}\gamma Gt$) (n.b., k covers both positive and negative values).

$$E(q,\Delta,k) = E_0(q,\Delta)e^{i2\pi(q+\Delta q)\Delta z_o} \times \int_{-\infty}^{\infty} \rho(z_o)e^{i2\pi\Delta q z_o}\, e^{i2\pi k z_o}\,dz_o \quad [21]$$

which gives

$$E(q,\Delta,z_o) = E_0(q,\Delta)\underbrace{e^{i2\pi(q+\Delta q)\Delta z_o}}_{\substack{\text{zeroth order}\\ \text{phase shift}}}\rho(z_o)\underbrace{e^{i2\pi\Delta q z_o}}_{\substack{\text{first order}\\ \text{phase shift}}}. \quad [22]$$

This is the one-dimensional projection image of the echo (this is closely related to the one-dimensional imaging calibration method given in Shape Analysis of the Spin Echo and One-Dimensional Images). It is because the phase shifts are resolved in Eq. [22] that $E_0(q,\Delta)$ can be recovered. If the signal-to-noise ratio is high, the spectrum can be resolved by autophasing, while for poorer signal-to-noise ratios, the absolute value of the spectrum must be taken, producing $E_0(q,\Delta)\rho(z_o)$. The signal averaging using absolute value spectra is, however, less efficient owing to the coaddition of noise and the absence of phase cycling (*21*). This phase-twist elimination process is nicely illustrated in Fig. 2 of Ref. 21.

When $k = -\Delta q$, Eq. [21] reduces to (n.b., the two exponential terms in the integral equal 1 and $\int\rho(z_o)\,dz_o = 1$, see Part 1, Eq. [29])

$$E(q,\Delta,k) = E_0(q,\Delta)e^{i2\pi(q+\Delta q)\Delta z_o} \quad [23]$$

and thus, at $t = -\Delta 2\pi q/(\gamma G)$, with respect to the echo center, the phase-twisted echo will cause a coherent superposition (whether this is before or after the echo center depends on the sign of the mismatch). Since $E_0(q, \Delta)$ can be recovered, it is possible to perform signal averaging even though Δq and Δz_o may fluctuate between scans. Obviously, t will vary as Δq fluctuates; consequently, the phase-twist analysis is performed after every scan.

Apart from the signal-to-noise problem, a further negative aspect of this method is that since signal acquisition occurs in the presence of a gradient, this method is not suitable for use with spectra containing more than one resonance; however, the serious gradient disturbances that warrant the use of MASSEY are normally associated only with measurements of large slowly diffusing species (e.g., polymers), and so spectral resolution is less likely to be an issue.

SAMPLE PREPARATION AND SPECTROMETER SETUP

Sample Preparation

The sample and, of course, the gradient probe itself should be firmly held inside the magnet with the sample maintaining a constant position with respect to the gradient coil former. The sample should be wholly contained inside the linear region of the gradient coils, and thus typically the sample is contained in a volume not more than 1 cm high. Such a sample, though, has large changes in magnetic susceptibility close to the rf coils. Accordingly, it is very difficult to achieve good resolution (i.e., difficult to shim). A solution is depicted in Fig. 12. This method, compared to just coaxially inserting a bulb into an NMR tube, has an advantage in that it is easy to clean the sample tube or work with viscous substances. It also gives a precise shape with no meniscus effect. Recently, two-piece susceptibility-matched microtubes and inserts have become commercially available. In passing, we note that instead of physically restricting the size of the sample, a slice-selective pulse (*55*) could be used to restrict the sample volume. However, this is possible only on more sophisticated spectrometers, where the diffusion gradients can be changed independently of the slice gradient. Furthermore, it should be noted that selective pulses are not of pure phase and do not have sharp cutoff frequencies.

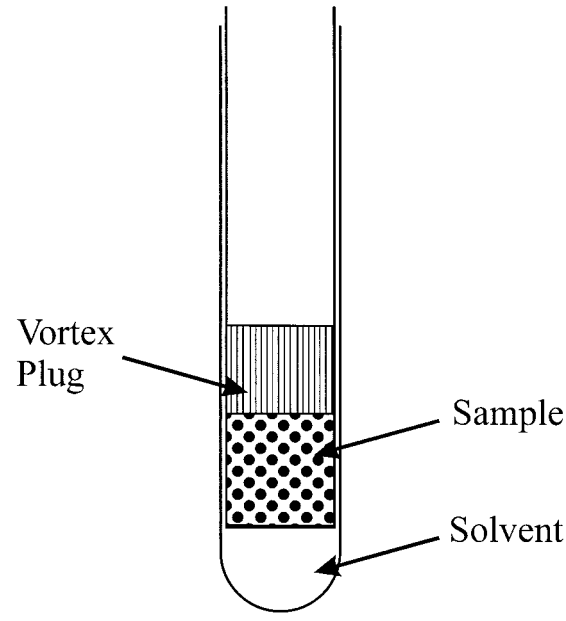

Figure 12 Ideally, all of the sample is contained within the constant region of the magnetic field gradient (see Fig. 3). Since the design of gradient coils are normally limited by the probe dimensions, it is generally necessary to keep the sample small so as to remain within the (small) volume of constant gradient. A simple solution is to place the sample in a cylindrical sample tube and then cap the sample with a vortex plug, ideally of the same magnetic susceptibility. This tube is then coaxially inserted into a tube containing either an NMR inert solvent with a similar magnetic susceptibility or the same solvent but without the solute of interest. Thus, the NMR-active part of the sample is short, whereas the sample is still magnetically long and allows easier shimming. A further advantage, especially of this arrangement of the sample, is that it helps to confine the sample to the region having the most homogeneous rf.

For very strong (in the NMR sense) samples (e.g., performing a diffusion measurement on pure water), radiation damping (*56*) can be a problem. Since the severity of the problem is related to the magnitude of the initial magnetization, one simple solution is to use a very small sample—for example, by placing the sample in a small spherical bulb (e.g., Wilmad cat. no. 529A).

B_0 Homogeneity and Field-Frequency Locking

If the sample in question has only one or at least well-separated resonances, a high degree of resolution is of little consequence as long as there is sufficient signal-to-noise. If it is necessary to use

a short sample to stay within the constant region of the gradient and susceptibility-matched microtubes or the like are unavailable, the process of shimming becomes very difficult. Furthermore, the initial line shape may be so poor that it is impossible to shim the sample using the lock signal (assuming that the sample contains a suitable deuterated compound). In such circumstances, it is easier to first shim the probe on a normal long sample and then iteratively shim and gradually reduce the volume of the sample to the (short) sample to be measured. After the first shimming of the long sample, the nonspinning shims (i.e., those without axial symmetry) should be largely correct, but owing to the shortness of the sample, the z and z^2 shims will require particular attention. It is common to have to use very large values for the z^2 shim. Particularly when the line shape is poor, it is generally easier to shim using the FID (*57*). Although spinning the sample helps to average out the effect of background gradients allowing a higher-resolution spectrum to be obtained, the spinning also causes motion in the sample. Consequently, the sample must not be spun in a diffusion experiment (see Sample Preparation). We note in passing, however, that a stop-and-go sample spinner suitable for use in PFG experiments has been developed that allows for the spinning to be arrested during the motion-sensitive part of the experiment, and yet spun to achieve higher resolution during acquisition (*58*).

Normally, the ^{2}H (or other suitable nucleus) lock is coupled to the z-shim coil to counteract the natural drift of the magnet. A gradient pulse will obviously affect this mechanism. The simplest solution is simply to turn the lock off. In fact, with spectrometers based on superconducting magnets, after resolution is achieved by shimming, running unlocked generally has almost no effect on resolution, and experiments requiring even high degrees of resolution can normally be performed as long as the duration of the experiment is not long with respect to the drift rate of the magnet. The situation is different with electromagnets, which are generally much more unstable. The best solution is just to gate the lock off before a gradient pulse and then to gate it on at the end of the pulse (ideally after the dissipation of any eddy current effects). In many modern spectrometers, such blanking procedures are a standard function of the electronics and pulse sequence programming.

Temperature Control and Calibration

The most convenient way of calibrating the sample temperature is to use some compound with temperature-dependent chemical shifts such as ethylene glycol or methanol (e.g., see Refs. *59–61*) or piezoelectric thermometers (*62*). However, it must be noted that the calibration technique using temperature-dependent chemical shifts is not perfect, and care must be taken in that the temperature control unit of most spectrometers is generally not very linear (Fig. 13). Typically, if the probe temperature is changed, at least 10 min must be allowed for the probe and sample temperature to reach equilibrium. The exact time required will be dependent on the probe, airflow, sample, and sample size. The calibration becomes more problematic when the sample has a high ionic strength and high-power proton decoupling is used (*63*).

SAMPLE PROBLEMS AND SOLUTIONS

Temperature Gradients and Convection

Since the temperature regulation in NMR probes is performed by heating air (or cold nitrogen gas) flowing in through the base of the probe (Fig. 4), it is possible for temperature gradients to be produced along the long axis of the sample. If the temperature gradient is large enough, convective flow will be induced along the long axis. (It is also reasonable to expect that transverse temperature gradients and convection could exist.) Assuming that the convective currents are planar along the z axis, the convection will transport equal amounts of the sample in opposite directions along the temperature gradient. Thus, whereas unidirectional flow simply causes a phase change of the signal but not an attenuation (see Part 1), convection results in attenuation (*4*, *64*). Hence, the effects of convection appear as an increase in the measured diffusion coefficient. The severity of the temperature gradient will also depend upon the efficiency of heat transfer and viscosity in the sample as well as the experimental factors (e.g., gas flow rate, geometry and size of the sample and interior dimensions of the probe, etc.).

The chemical shift of the ^{59}Co resonance of the (very symmetric) complex $K_3Co(CN)_6$ has an extremely large temperature dependence (1.45 ppm K^{-1}) and is thus a suitable compound for investigating the presence of thermal gradi-

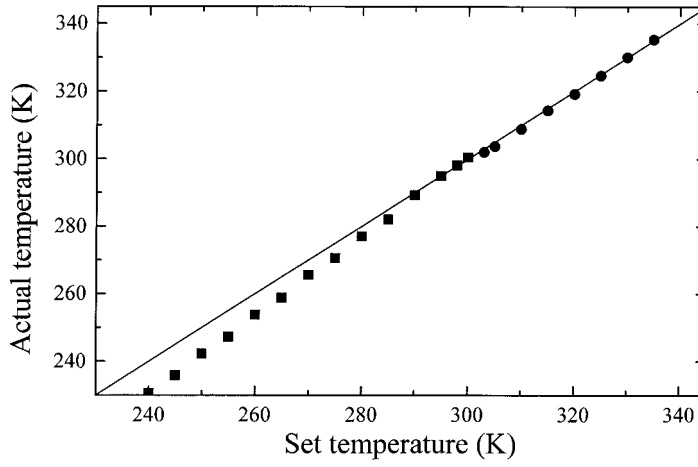

Figure 13 An example of a temperature calibration plot for a 5-mm multinuclear inverse probe for a (standard bore) Bruker DRX 300 Spectrometer. Generally, the set and actual temperatures correspond well around ambient temperature using methanol (closed squares) and ethylene glycol (closed circles). Note the kink between the temperature measured with methanol and ethylene glycol. This results from imperfect calibration of the chemical shifts of these compounds with respect to temperature. The solid line represents the ideal case of perfect correspondence between the set and actual temperature. The correlation between the two temperatures can be improved by increasing the flow rate of the cooling/heating gas and moving the thermocouple closer to the sample (see, for example, Fig. 4). However, shimming generally becomes more problematic as the thermocouple becomes closer to the sample.

ents (*65*). The thermal gradient, ∇T, can be estimated directly from the linewidth,

$$\nabla T(\mathrm{K\ cm^{-1}}) = \frac{\text{linewidth (ppm)}}{1.45 \times \text{rf coil height (cm)}} \quad [24]$$

The most fundamental means for minimizing convection problems is to have good temperature control, which to some extent is generally improved by increasing the airflow, although this will depend strongly on the probe construction (e.g., the separation between the outside of the sample and the insert glass in the probe). Convection is also reduced through the use of short and narrow samples, since the walls retard the onset of convective flow. If convection is still a problem, modified PFG diffusion sequences which rely upon gradient moment nulling (*64*) can be used. To see how this method works, it is necessary to understand the connection between flow and phase. The phase shift at time t of a nuclear spin following a path $\mathbf{r}(t')$ in a gradient $\mathbf{g}(t')$ is given by

$$\phi(t) = \gamma \int_0^t \mathbf{g}(t') \cdot \mathbf{r}(t')\, dt' \quad [25]$$

Only the component of the spin's motion in the direction of the gradient, $z(t)$, is relevant, and this can be expanded in a Taylor series (*66*)

$$z(t) = z_0 + \left(\frac{\partial z}{\partial t}\right)_{t=0} t + \frac{1}{2}\left(\frac{\partial^2 z}{\partial t^2}\right)_{t=0} t^2 + \cdots \quad [26]$$

The terms on the right-hand side of Eq. [26] correspond to the position z_0, velocity $v_0 = (\partial z/\partial t)_{t=0}$ and acceleration $a_0 = (\partial^2 z/\partial t^2)_{t=0}$, etc., and thus, Eq. [25] can be rewritten as

$$\phi(t) = \gamma z_0 M_0 + \gamma v_0 M_1 + \frac{1}{2}\gamma a_0 M_2 + \cdots \quad [27]$$

where

$$M_n = \int_0^t g_z(t')(t')^n\, dt' \quad [28]$$

M_n is termed the nth moment of $g_z(t)$ with respect to t (n.b., this should not be confused with macroscopic magnetization). Equation [27] provides the basis of so-called gradient moment

nulling methods and flow compensation. In the present analysis, it is assumed that the convection current has a constant laminar flow in the z direction during the pulse sequence; thus, this method does not compensate for turbulent convection. An example of a flow-compensated double-stimulated echo sequence (*64*) is shown in Fig. 14. The signal attenuation due to diffusion for this sequence is given by (*64*)

$$E = \exp\left(-\gamma^2 g^2 D\delta^2\left(t_d + \frac{4\delta}{3} + 2\tau_g\right)\right) \quad [29]$$

where t_d and τ_g are defined in Fig. 14. For completion, we note that by nulling higher moments, second-order effects (i.e., flow acceleration), etc., can be eliminated.

Short Relaxation Times, Internal Gradients, and Other Problems

Short Relaxation Times. From inspection of Fig. 1, we can see that the maximum and minimum possible values of Δ are given by

$$\Delta_{max} = 2\tau - \delta - \left(\frac{\pi}{2}\right)_{rf} \quad [30]$$

$$\Delta_{min} = \delta + (\pi)_{rf} \quad [31]$$

where $(\theta)_{rf}$ means the duration of the θ pulse. In Eq. [30], we have asssumed that the τ period begins halfway through the $\pi/2$ rf pulse, and in Eq. [31] we have corrected for the length of the π pulse. With the exception of Carr-Purcell-Meiboom-Gill (CPMG)-like sequences, however, the duration of the rf pulses are insignificant to the length of δ and Δ, and we will henceforth neglect corrections for the rf pulses in our discussion. As can be realized from our discussion on eddy currents above (Eddy Currents and Perturbation of B_0), Δ_{max} as defined by Eq. [30] and Δ_{min} as defined by Eq. [31] are in reality unusable, since additional delays between the end of the first gradient pulse and the π pulse and between the second gradient pulse and acquisition are needed to allow settling of the side effects induced by the gradient pulses.

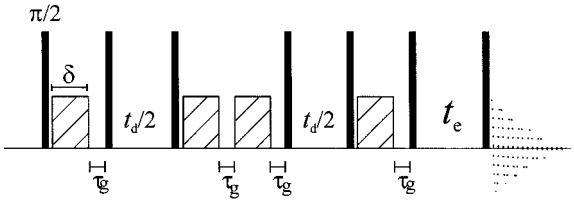

Figure 14 A double-stimulated echo sequence that is compensated for flow including an LED delay, t_e (*64*). The sequence refocuses all constant-velocity effects. The first moment of the effective gradient over the whole sequence is zero. The phase cycling for this sequence can be found in Ref. *64*.

Although E does not explicitly include τ, experimentally the largest usable Δ will be determined by the maximum usable value of τ, which is, of course, related to the spin–spin relaxation time (i.e., T_2) of the species that we are measuring. When studying species for which $T_1 \gg T_2$ (e.g., macromolecules), it is advantageous to use the stimulated echo sequence [Fig. 8(A)], since the delays in the pulse sequence can be chosen so that the magnetization is "stored" along the z axis for most of Δ. In calculating the echo attenuation, it is possible to use the peak height if the line shape is Lorentzian, but the integral of the resonance is to be preferred. A further advantage of the stimulated echo sequence is that complications resulting from J modulation (see J Modulation) can be reduced by keeping τ_1 small. However, the negative aspect of the stimulated pulse sequence is that while for the Hahn spin-echo-based sequence we have

$$S(2\tau)_{g=0} = S(0)\exp\left(-\frac{2\tau}{T_2}\right) \quad [32]$$

for the stimulated echo (STE) sequence we have

$$S(2\tau)_{g=0} = \frac{S(0)}{2}\exp\left(-\frac{2\tau_1}{T_2} - \frac{\tau_2}{T_1}\right) \quad [33]$$

The additional loss of a factor of 2 arises because the second 90° pulse stores only the y component of the magnetization (2). Thus, the STE sequence will be advantageous only when $T_1 \gg T_2$, keeping τ_1 only long enough to contain the gradient pulse and as short as possible for the dissipation of any eddy currents. Some example plots comparing Eqs. [32] and [33] are given in Fig. 15.

An important point to be realized is that short T_2 relaxation times, especially with nonquadrupolar nuclei, are often due to the presence of inter-

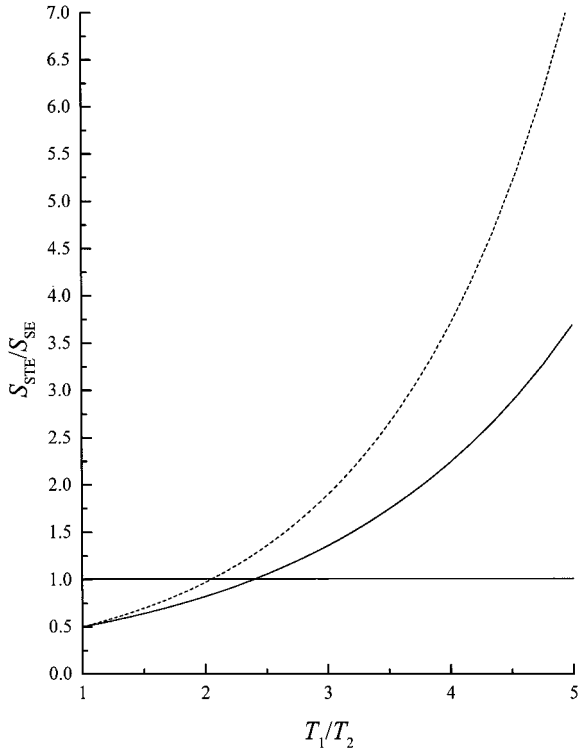

Figure 15 The ratio of the signal obtained from the stimulated echo (STE) sequence to that obtained from the Stejskal and Tanner spin-echo (SE) sequence versus T_1/T_2 in the absence of gradients. The simulations were calculated using Eqs. [32] and [33]. In performing these simulations, we have assumed that $2\tau = T_1$ in the case of the Stejskal and Tanner sequence and that $2\tau_1 + \tau_2 = T_1$ in the case of the STE sequence. The simulations were performed for the cases of $\tau_1 = \tau_2/2$ (—) and that $\tau_1 = \tau_2/4$ (----). The solid horizontal line indicates the boundary above which the STE sequence gives better signal-to-noise than the Stejskal and Tanner sequence. As expected, when $T_1/T_2 = 1$, the stimulated echo sequence gives only half the intensity of the spin-echo sequence.

nal magnetic gradients and are not an inherent property of the species being measured (i.e., T_2^* and not T_2). Thus, in addition to simply using the STE sequence, benefit may be had by using specialized sequences to counteract the effects of the internal gradients, and these form the subject of the following subsection.

Internal Gradients. Ideally, the only magnetic gradients present during the performance of a PFG sequence would be the purposely applied constant gradients. In practice, the B_0 field is never perfect (e.g., imperfect shimming and the proximity of the thermocouple to the sample) and nonhomogeneous internal gradients are common within many samples (e.g., red blood cells, metal hydrides, colloids, and porous media) owing to differences in magnetic susceptibility. For example, it is estimated that red blood cells have gradients up to 2×10^{-2} T m^{-1} (*67*, *68*). Even minute air bubbles in an apple can lead to large background gradients (*69*). In fact, in hydride samples, such internal gradients can be of the order of 0.5 T m^{-1} (*70*). In this section, we consider the effects of constant and nonconstant (i.e., nonuniform) background gradients (i.e., nonuniform both in direction and magnitude throughout the sample) on diffusion measurements. These background gradients result in a decrease in the observed T_2 through the effects of translational diffusion of nuclear spins (*71–79*). This can be easily understood by considering the effects of a gradient on the Hahn spin-echo sequence (see the discussion below), although in fact there is no exact theory for treating the effects of diffusion in a general nonuniform gradient (*76*).

Let us begin our investigation of the effect of background gradients by considering the Stejskal and Tanner sequence, but in the presence of a uniform constant background gradient of strength $\mathbf{g}_0$ (Fig. 16). Using the theory developed in the first article (see Part 1, The Macroscopic Approach, and the Maple program in the Appendix) to calculate the diffusion related part of the attenuation, we can derive the echo signal amplitude including the effects of the background

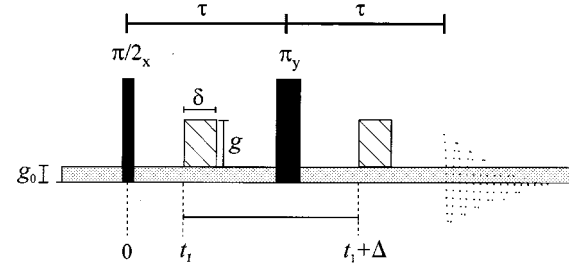

Figure 16 The Stejskal and Tanner Pulse sequence in the presence of a background gradient $\mathbf{g}_0$. Simplistically, it is assumed that the background gradient is uniform in magnitude and direction throughout the entire sample during the sequence.

gradients for the Stejskal and Tanner sequence (Table 6) to be (*49*)

$$S(2\tau) = S(0)\exp\left(\frac{-2\tau}{T_2}\right)\exp\Bigg(\underbrace{-\gamma^2 g_0^2 D\frac{2}{3}\tau^3}_{\mathbf{g}_0\text{ term}} \underbrace{-\gamma^2 g^2 D\delta^2(\Delta - \delta/3)}_{\mathbf{g}\text{ term}} + \underbrace{\gamma^2 \mathbf{g}\cdot\mathbf{g}_0 D\delta\left[t_1^2 + t_2^2 + \delta(t_1 + t_2) + \frac{2}{3}\delta^2 - 2\tau^2\right]}_{\mathbf{g}\cdot\mathbf{g}_0\text{ cross-terms}}\Bigg) \quad [34]$$

where $t_2 = 2\tau - (t_1 + \Delta + \delta)$. Some important points can be understood by considering Eq. [34] in detail. The $\mathbf{g}_0$ term in Eq. [34] is simply the attenuation factor for a Hahn spin-echo sequence in the presence of a constant gradient (see Part 1, Eq. [17]); the $\mathbf{g}$ term is the usual PFG diffusion attenuation term (see Eq. [1]), while the final (interference) term represents the coupling between the applied and background gradients. If, as usual, τ is kept constant and the $\mathbf{g}_0$ term is included in $S(2\tau)_{g=0}$, then from Eq. [34] we can define the signal attenuation as

Table 6 Time Dependence of the Applied and Background Gradient for the Stejskal and Tanner Pulse Sequence (see Fig. 16)

Subinterval of Pulse Sequence	$\mathbf{g}(t)$
$0 < t \le t_1$	g_0
$t_1 < t \le t_1 + \delta$	$g_0 + g$
$t_1 + \delta < t \le t_1 + \Delta$	g_0
$t_1 + \Delta < t \le t_1 + \Delta + \delta$	$g_0 + g$
$t_1 + \Delta + \delta < t \le 2\tau$	g_0

$$E(2\tau) = \frac{S(2\tau)_{g=0}\exp\left(-\gamma^2 g^2 D\delta^2(\Delta - \delta/3) + \gamma^2 \mathbf{g}\cdot\mathbf{g}_0 D\delta\left[t_1^2 + t_2^2 + \delta(t_1 + t_2) + \frac{2}{3}\delta^2 - 2\tau^2\right]\right)}{S(2\tau)_{g=0}}$$

$$= \exp\left(-\gamma^2 g^2 D\delta^2(\Delta - \delta/3) + \gamma^2 \mathbf{g}\cdot\mathbf{g}_0 D\delta\left[t_1^2 + t_2^2 + \delta(t_1 + t_2) + \frac{2}{3}\delta^2 - 2\tau^2\right]\right). \quad [35]$$

If the condition $\mathbf{g}\delta \gg \mathbf{g}_0\tau$ (or $\mathbf{g}\delta \gg \langle\mathbf{g}_0^2\rangle^{1/2}\tau$ if $\mathbf{g}_0$ is nonconstant) holds, then the $\mathbf{g}_0$ and $\mathbf{g}\cdot\mathbf{g}_0$ terms can be neglected and Eq. [34] (or Eq. [35]) reduces to Eq. [2] (*70*). By comparing Eq. [35] with Eq. [2], and considering the case of a homogeneous isotropically diffusing species, we see that E now depends not only on δ and Δ but also on the duration of the other delays in the pulse sequence. Furthermore, while in the absence of $\mathbf{g}_0$ a plot of $\ln(E)$ versus $\gamma^2 g^2 \delta^2 \Delta$ (i.e., $q^2\Delta$) is linear, in the presence of $\mathbf{g}_0$, the plot will be curved owing to the $\mathbf{g}\cdot\mathbf{g}_0$ term (*77*). Interestingly, the overall sign of the $\mathbf{g}\cdot\mathbf{g}_0$ term will depend on the relative direction between the applied and internal gradients (recall that $\mathbf{g}\cdot\mathbf{g}_0 = gg_0\cos\alpha$, where α is the angle between g and g_0). Thus, by reversing the polarity of the applied gradient, the effect of static field homogeneity can be tested (*80*). However, if there is a distribution of background gradients, reversing the polarity of the applied gradient would only affect the signal amplitude if the distribution of $\mathbf{g}_0$ were not symmetric about $g_0 = 0$ (*70*, *81*). Furthermore, measured (i.e., apparent) anisotropic diffusion could result from anisotropic background gradients owing to the $\mathbf{g}\cdot\mathbf{g}_0$ term (*82–84*). We note that this type of problem can also result from cross-terms between the diffusion and imaging gradients in imaging pulse sequences involving diffusion measurements (*85*).

Performing a similar calculation for the signal amplitude for the STE sequence [Fig. 8(A)] in-

cluding the presence of a background gradient, we obtain (*45*, *86*)

$$S(2\tau) = \frac{S(0)}{2}\exp\left(-\frac{2\tau_1}{T_2} - \frac{\tau_2}{T_1}\right)\exp\left(\underbrace{-\gamma^2 g_0^2 D\frac{2}{3}\tau_1(\tau_2 + 2\tau_1/3)}_{\mathbf{g}_0 \text{ term}} \underbrace{-\gamma^2 g^2 D\delta^2(\Delta - \delta/3)}_{\mathbf{g} = 0 \text{ term}} + \underbrace{\gamma^2 \mathbf{g}\cdot\mathbf{g}_0 D\delta\left[t_1^2 + t_2^2 + \delta(t_1 + t_2) + \frac{2}{3}\delta^2 - 2(\tau_1 + \tau_2)\tau_1\right]}_{\mathbf{g}\cdot\mathbf{g}_0 \text{ cross-terms}}\right) \quad [36]$$

where $t_2 = \tau_1 - \delta - t_1$. The same simplifications can be applied as in the case of Eq. [34]. By comparing Eqs. [34] and [36], and by realizing that the duration τ in the Stejskal and Tanner sequence is generally much longer than τ_1 in the STE sequence, it can be seen that the last term in Eq. [36] (i.e., $2(\tau_1 + \tau_2)\tau_1$) is much smaller than the corresponding term in Eq. [34] (i.e., $2\tau^2$); thus, the effect of the cross-term $\mathbf{g}\cdot\mathbf{g}_0$ is smaller for the STE sequence (*86*). As an aside, we note that the effects of background gradients can, of course, also be included with the shaped gradient pulse versions of the Stejskal and Tanner sequences given in Modulated Gradients, or similarly with the STE sequence.

In the case of nonuniform gradients, when the equality $\mathbf{g}\delta \gg \langle \mathbf{g}_0^2\rangle^{1/2}\tau$ is not met, the interpretation of Eq. [34] (or [36]) becomes very difficult (*70*, *87*). If the distribution of $\mathbf{g}_0$ is symmetric about $g_0 = 0$ and not too large, a series expansion can be used to correct for the background gradients (*81*). Perhaps counterintuitively, the measured diffusion in the presence of internal gradients is often found to be lower than the actual diffusion coefficient (*87*, *88*). The reason for this is the following. The measured diffusion is in essence an ensemble average, and the internal gradients will weight this distribution at the time of signal acquisition, since the degree of dephasing caused by the internal gradients is a function of the diffusivity. The faster diffusing spins will be more attenuated, and consequently it is the more slowly diffusing spins that contribute most to the echo signal (*87*). This is analogous to the effect found for spins diffusing in a restricted geometry having an absorbing wall (*89*). Since the attenuation due to the background gradients may be indistinguishable from the attenuation due to the applied gradient, the effects of background gradients can be mistaken for restricted diffusion (*75*).

The basis of most sequences for the removal of the $\mathbf{g}_0$ term is to add additional π pulses to the PFG sequence to refocus the dephasing effects of $\mathbf{g}_0$ in a way analogous to the CPMG sequence (*90*). Clearly, such sequences must be designed with an odd number of π pulses between the gradient pulses, since an even number of pulses would simply result in the effects of the second gradient pulse adding to the dephasing effects of the first gradient pulse (*90*). However, removal of the $\mathbf{g}\cdot\mathbf{g}_0$ cross-term is more problematic. As noted above, one solution to the background gradient problem is to use applied gradients that are much larger than the background gradients. When this is not possible, more sophisticated pulse sequences must be used. In 1980, Karlicek and Lowe (*91*) proposed the use of alternating (bipolar) pulsed-field gradients in a modified Carr–Purcell sequence [Fig. 17(A)] to eliminate the contribution of the $\mathbf{g}\cdot\mathbf{g}_0$ cross-term, since the number of positive $\mathbf{g}$ intervals equals the number of negative $\mathbf{g}$ intervals. The attenuation due to diffusion for the Karlicek and Lowe sequence can be calculated using the theory developed in the first article (see Part 1, The Macroscopic Approach) to be (*91*)

$$E(g, 2n\tau) = \exp\left(-\frac{2}{3}\gamma^2 D\left[n\mathbf{g}_0^2\tau^3 + (n-1)^3 \times \mathbf{g}^2\left(\tau - \frac{(\delta_1 + \delta_2)}{2}\right)^2 \times \left(\tau + \frac{(\delta_1 + \delta_2)}{(n-1)^2}\right)\right]\right) \quad [37]$$

where the integer n, δ_1, and δ_2 are defined in Fig. 17(A). Systematic errors due to the cross-term can also be eliminated in a Carr–Purcell se-

quence that uses only pulses of one polarity (*70*), but this sequence is not as efficient as that of Karlicek and Lowe, especially when $T_2 < T_1$. The Karlicek and Lowe sequence (*91*) is limited by T_2, and thus it is desirable to have STE-based pulse sequences. Cotts and coworkers (*92*) presented three modified STE sequences incorporating alternating pulsed-field gradients [Fig. 17(B)] which greatly reduce the effects of the background gradients. Latour et al. (*77*) proposed a pulse sequence that combines features of the Karlicek and Lowe and Cotts pulse sequences in which the gradient pulses in the normal STE echo pulse sequence are replaced by a series of short gradient pulses of alternating sign [Fig. 17(C)]. Van Dusschoten and coworkers (*86*) proposed a new variation termed the PFG multiple-spin-echo (PFG MSE) pulse sequence [Fig. 17(D)]. For this sequence, the echo attenuation is described by (n.b., the similarity to Eq. [34]),

$$S(2\tau) = S(0)\exp\left(\frac{-2n\tau}{T_2}\right)\exp\left(\underbrace{-\gamma^2 g_0^2 D\frac{2}{3}n\tau^3}_{\mathbf{g}_0\text{ term}} \underbrace{-\gamma^2 g^2 D\delta^2(\Delta - \delta/3)}_{\mathbf{g}\text{ term}} + \underbrace{\gamma^2 \mathbf{g}\cdot\mathbf{g}_0 D\delta\left[t_1^2 + t_2^2 + \delta(t_1 + t_2) + \frac{2}{3}\delta^2 - 2\tau^2\right]}_{\mathbf{g}\cdot\mathbf{g}_0\text{ cross-terms}}\right) \quad [38]$$

where n denotes the number of π pulses. They noted that by setting $\frac{2}{3}\delta^2 \approx 2\tau^2$, the effects of the background and internal gradients can be largely removed.

J Modulation

Coupled homonuclear spin systems present special problems for performing PFG diffusion measurements. During the echo sequences used for measuring diffusion, the precession frequencies, and thus the refocusing, depend on the magnitude of the spin coupling constant, J. Furthermore, the rf pulses exchange the spin states of the coupled nuclei. For a coupled pair of nuclei, echo maxima occur when

$$\tau = n/J \quad [39]$$

and negative maxima occur when

$$\tau = n/(2J) \quad [40]$$

where J is in hertz and n is an integer. Thus, when performing a PFG experiment, it is important to consider the pulse sequence delays with respect to J to obtain good signal-to-noise ratios. With the STE sequence, it is preferable to keep $\tau_1 \ll 1/J$.

It is also worth noting that when working with coupled systems, decoupling can cause anomalous changes in signal intensity, especially in systems with large coupling constants. This effect results from incomplete decoupling during gradient pulses. For example, if the Stejskal and Tanner sequence is used to measure the diffusion coefficient of the hypophosphite ion ($H_2PO_2^-$) for which $J_{PH} = 141$ Hz, it is advisable to gate the broadband proton decoupling off during the τ periods and to gate it on only during the recycle delay and during the acquisition of the ^{31}P signal. In this way, most of the NOE enhancement is maintained, and yet there is no distortion of the phase distributions in either of the τ periods during the gradient pulses.

Cross Relaxation

Another problem which is in some ways obvious is that of cross-relaxation when performing diffusion measurements of macromolecular systems (*93*). The problem can be understood as follows. Consider that we are measuring the diffusion of water in a macromolecule solution using the STE pulse sequence. After the first $\pi/2$ pulse, both the macromolecule and water magnetization are in the x–y plane. For simplicity, we assume that

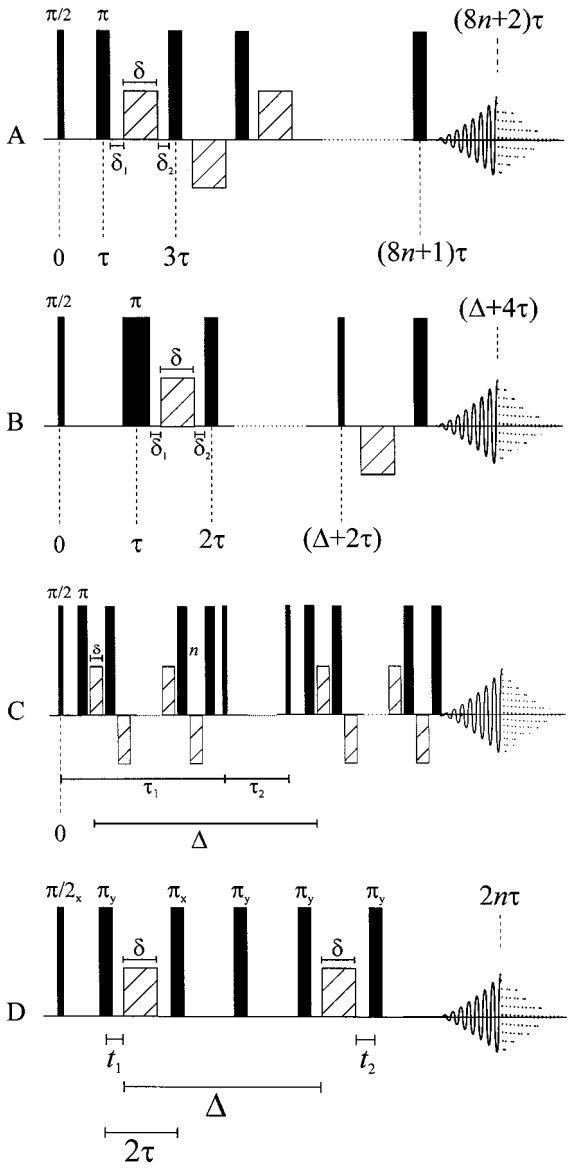

Figure 17 Sequences for removal of background gradients. (A) The Karlicek and Lowe sequence (*91*), (B) the nine pulse sequence of Cotts et al. (*92*), (C) the improved stimulated echo sequence of Latour et al. (*77*), and (D) the PFG multiple-spin-echo (PFG MSE) pulse sequence of Van Dusschoten et al. (*86*).

the T_2 relaxation time of the macromolecule is much less than that of the water so that by the end of the τ_1 period the macromolecules are fully relaxed, whereas the relaxation of the water magnetization is insignificant. After the application of the second $\pi/2$ pulse, the z magnetization of the macromolecule will be zero, since it was entirely aligned along the z axis prior to the pulse. For the water magnetization, the situation is entirely different; after the pulse, the water magnetization is proportional to $\cos(qz)$, where $q = (2\pi)^{-1}\gamma\delta g$ [recall that the gradient pulse creates a helix along the direction of the gradient with a period of $2\pi/(\gamma\delta g)$]. However, as qz ranges over many periods, the net z magnetization over the sample is zero. Thus, the local normalized deviation from equilibrium in the macromolecule phase will be -1, and for the water phase, $\cos(qz) - 1$. Thus, during τ_2, cross-relaxation results from the equilibrium differences in both phases. Consequently the cross-relaxation rate will depend on q. Equations have been derived to account for this cross-relaxation in a two-phase system (*93*). If significant cross-relaxation occurs, it can affect the measured signal intensities, thereby complicating diffusion measurements. Under limited conditions, it is possible to determine the exchange parameters to allow D to be calculated correctly. Importantly, the problem of cross-relaxation does not apply to the Stejskal and Tanner sequence.

Multiple Quantum and Heteronuclear Experiments

It is often desirable to work with heteronuclei, especially when measuring the diffusion coefficient of nuclei in a complex mixture such as a biological fluid. However, heteronuclei generally have a sensitivity far beneath that of protons. Further, because of the low gyromagnetic ratios of heteronuclei, larger gradients must be used. The most straightforward means of alleviating the signal-to-noise problem is through the use of specifically labeled/enriched probe molecules. Large gains in sensitivity can be made through using pulse sequences to generate polarization transfer from protons to the heteronuclei (*94*, *95*). This approach has the advantage of generating multiple quantum transitions. Multiple quantum transitions can, of course, also be used in homonuclear work (*96*, *97*). Multiple quantum spectra are also generally simpler and better resolved than the corresponding single quantum spectra; and for n coupled protons, the n-quantum transition is free of dipolar couplings. This may also allow an increase in the possible observation time owing to decreased relaxation (*98*). Furthermore, in the case of homonuclear studies, multiple quantum spectra have the added benefit of providing solvent suppression. However, there are some restrictions on the applicability of multiple quantum PFG experiments, since the spectrum of the species in question must have either a scalar, dipolar, or quadrupolar coupling (e.g., Refs.

94–99). If the attenuation of the multiple quantum coherence can be studied (instead of the single quantum coherence), the same degree of attenuation can be achieved, but with smaller gradients and therefore smaller eddy current problems. In multiple quantum experiments, it is the effective sum of the γ values of the nuclei involved in the coherence which is relevant to the attenuation. Thus, for the Stejskal and Tanner pulse sequence, in the case of free diffusion and neglecting the effects of background gradients, the formula relating echo signal attenuation to diffusion can be written as

$$E(q, \Delta) = \exp(-f(\gamma)g^2D\delta^2(\Delta - \delta/3)). \quad [41]$$

For the normal (i.e., single quantum) experiment, $f(\gamma) = \gamma^2$. For homonuclear multiple quantum experiments, $f(\gamma) = (n\gamma)^2$. Examples of multiple quantum pulse sequences based on the Stejskal and Tanner and STE sequences are presented in Fig. 18. For heteronuclear multiple quantum experiments, the definition of $f(\gamma)$ is not as straightforward. For heteronuclear double quantum experiments with an IS spin system, where I (not to be confused with I, the current) is the observed nucleus, $f(\gamma) = ((\gamma_1 + \gamma_s)/\gamma_s)^2\gamma_1$ (*95*).

The use of heteronuclear inverse DEPT- (i.e., inverse detection) and IHETCOR-based sequences has been investigated (*94*, *95*). The DEPT-based sequence has significant advantages for working with low γ nuclei owing to the polarization transfer from the I spin (usually ^{1}H) to the S spin, whereas the IHETCOR pulse sequence is more suited to the observation of protons as the unfavorable polarization transfer from the less abundant heteronuclear population to the proton population. Coherence-order selection may be incorporated into the diffusion experiment to provide solvent suppression.

In the case of quadrupolar nuclei, if the spectrum contains a static quadrupolar splitting, the PFG experiment can be performed using a quadrupolar echo instead of a spin-echo (i.e., the π pulse would be replaced by a $\pi/2$ pulse in Fig. 1 and appropriate phase cycling) (*80*, *100*, *101*).

GRADIENT CALIBRATION

So far in our discussion, we have implicitly assumed that the value of the gradient is known. The reality is that before we can determine the diffusion coefficient, we need to determine the gradient strength very accurately (n.b., the gradient is squared in Eq. [2]). We now consider the different ways in which the gradient can be calibrated, although it should be noted that even without calibration the relative diffusion coefficients can be measured. The methods of gradient calibration are summarized in Table 7.

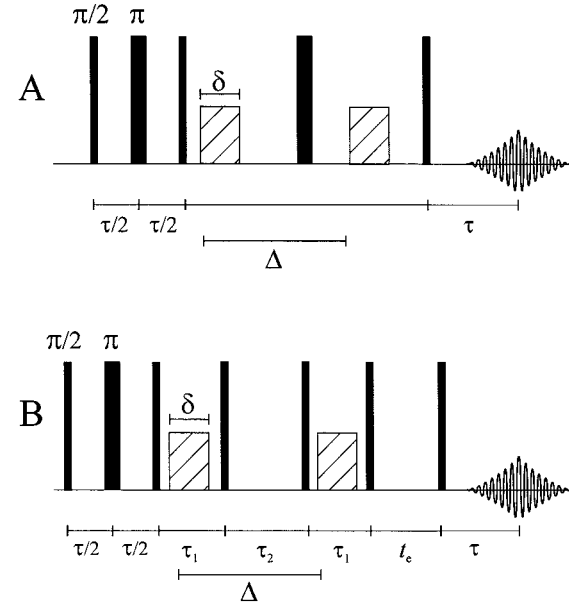

Figure 18 Some representative multiple quantum PFG sequences based on (A) the Stejskal and Tanner, and (B) the STE sequence. The phase cycling for these sequences can be found elsewhere (*96–99*).

Theoretical Coil Calculation

In theory, the applied gradient could be calculated from the known dimensions, geometry, number of turns of wire in the coil, and current applied (see Gradient Coils). In practice, this method should give an estimate with an error of $\leq 10\%$. The major reason is interaction with nearby metal in the probe and nonideal gradient pulse generation problems. Thus, other methods are needed to get accurate gradient calibrations.

A Standard Sample with Known Diffusion Coefficient

The simplest way of calibrating a gradient is to use a standard sample of known diffusion coefficient (e.g., pure water). Ideally, a reference compound should have a diffusion coefficient and T_2 that are not strongly temperature dependent. Some suitable standard samples and their diffu-

Table 7 Summary of Gradient Calibration Methods

Method	Range of Application	Pros/Cons
Coil calculation	Unlimited	+ Generally applicable − Can be complicated to perform − Not very accurate
Echo shape	$\gamma gl/2\pi <$ receiver bandwidth signal-to-noise	+ Generally applicable − Numerous systematic errors
1D Image	$\gamma gl/2\pi <$ receiver bandwidth signal-to-noise	+ Generally applicable + Information on gradient linearity
Gradient pulse mismatch	Similar to echo shape	Similar to echo shape
Standard sample	Need to have a relevant standard	+ Simple + Includes gradient non-ideality − Few suitable and accurate standards − Need accurate temperature control

sion coefficients are listed in Table 8. Apart from sample-dependent problems, the effects of eddy currents and/or mechanical vibrations, if present, will result in this method giving only an apparent calibration. If the sample experimental conditions (i.e., sample shape, delays, pulse lengths, gradient strengths, etc.) are used in a subsequent experiment, this calibration procedure has the advantage of automatically including nonideal gradient behaviour. However, because eddy current effects increase with gradient strength, a calibration at one current value cannot be used to determine the gradient strength at another value of the applied current. This method of gradient calibration is further limited by the need to have a compound containing a nucleus that can be observed with the probe at hand and with a similar diffusion coefficient and excellent temperature control. Clearly, a multinuclear probe gives the most possibilities. For lower diffusion coefficients, suitable reference compounds become more scarce. Glycerol has often been used as a reference, but its diffusion coefficient is greatly affected by water content as well as a highly temperature-dependent diffusion coefficient and T_2 (*4*, *102*).

Shape Analysis of the Spin-Echo and One-Dimensional Images

It is possible to calculate the gradient strength using the echo shape from a sample of known geometry. This is easy to understand if you consider that in the absence of a gradient there is no spatial dependence of the resonance frequency, but in the presence of a gradient there is a spatial dependence. Thus, the observed FID and spectrum will reflect both the gradient and the shape

Table 8 Some Selected Reference Compounds and Their Diffusion Coefficients at 298 K Useful for Calibrating PFG Experiments

Observe Nucleus	Compound	Diffusion Coefficient ($m^2\ s^{-1}$)	Reference
^{1}H	H_2O	2.30×10^{-9}	(*118*, *119*)
^{2}H	$^{2}H_2O$	1.87×10^{-9}	(*120*)
	$HO^{2}H$ in $^{2}H_2O$	1.90×10^{-9}	
^{7}Li	LiCl (0.25 M) in H_2O	9.60×10^{-10}	(*102*)
^{13}C	C_6H_6	2.21×10^{-9}	(*81*)
^{19}F	C_6H_6F	2.40×10^{-9}	(*102*)
^{21}Ne	Ne (4 MPa) in $^{2}H_2O$	4.18×10^{-9}	(*121*)
^{23}Na	NaCl (2 M) in H_2O	1.14×10^{-9}	(*122*)
^{31}P	$(C_6H_5)_3P$ (3 M) in C_6D_6	3.65×10^{-10}	(*102*)
^{129}Xe	Xe (3 MPa) in H_2O	1.90×10^{-9}	(*123*)
^{133}Cs	CsCl (2 M) in H_2O	1.90×10^{-9}	(*102*)

A more comprehensive listing can be found in Holz and Weingärtner (*102*).

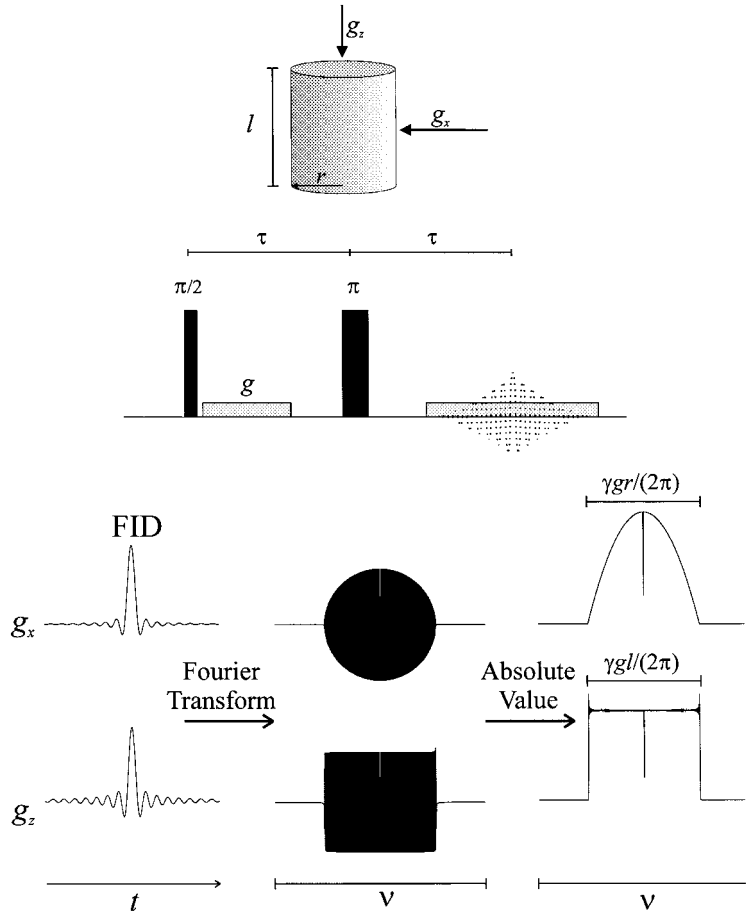

Figure 19 Schematic diagram of the cylindrical sample of length l and radius r used for determining the gradient strength and of the Hahn spin-echo sequence incorporating a read gradient of strength g used for obtaining a one-dimensional image of the sample. In the lower half of the figure, two simulated FIDs are given for the case of g_x (upper) and g_z (lower). The FID for the g_x case has the characteristic Bessel function profile (see Eq. [58]), whereas the FID acquired in the presence of g_z has a sinc function profile (see Eq. [72]). In both cases, it is possible to determine the strength of the gradient by analyzing the FID shape (e.g., from the zeroes of the Bessel function in the case of g_x). However, the Fourier transforms of both FIDs are more informative and easier to understand (e.g., the transforms return images of the sample cross-sections with respect to the gradient directions). The Fourier transforms are rapidly oscillating functions (these spectra appear dark owing to the printing resolution) with sharp frequency cutoffs in both cases. The power spectrum makes the cutoff easier to visualize (right-hand spectra). The width (ν) (Hz) of the spectra is $\gamma gr/2\pi$ and $\gamma gl/2\pi$ for the spectra acquired with g_x and g_z, respectively. The power spectra were calculated numerically from the simulated FID (not from Eqs. [65] and [83]) which was slightly truncated at the ends; hence, the oscillations at the top of the absolute value of the transform of the sinc function and also the dip in the middle of both. Experimentally, the FIDs are often more seriously truncated, and as a consequence, the oscillation artifacts are more pronounced. As the number of points used in the transform decrease, the edges of the absolute value spectra are not as sharp. Furthermore, if the echo is not quite in the middle of the acquisition, the transformed spectrum appears to have strange phasing; however, the absolute value spectrum solves the problem.

of the sample. Let us demonstrate with the case of a gradient with a right cylindrical sample of length l and radius r (Fig. 19), which is likely to be the most commonly used sample geometry. First, we will derive the shape of the echoes; then we will discuss the performance of such a measurement. We note in passing that the analysis has also been done for other geometries (*31*). It is unnecessary to follow the maths in the following two subsections; the main results are given by Eqs. [58] and [65] in the next subsection, and Eqs. [72], [83], and [84] in the following subsection. Part of the purpose of the derivations is to allow interested readers to more easily follow the seminal paper of Carr and Purcell (*27*), since these equations recur widely in the literature.

Case 1: Gradient Directed Across the Cylinder. We first consider the case of the gradient directed across a right cylindrical sample (*27*, *28*, *103*), i.e., $g = g_x$. This geometry has particular relevance to a spectrometer based on an electromagnet where the cylindrical axis would be along the z axis and the gradient would be directed along the x axis. Starting from Eq. [7], we can define the phase distribution of spins starting at x_0

$$P(\phi) = g(\phi_1)h(x_0) \qquad [42]$$

where

$$\phi = \phi_1 + \gamma g(2\tau - t) \qquad [43]$$

$$g(\phi_1) = \frac{1}{\sqrt{2\pi\langle\phi_1^2\rangle_{av}}} e^{-\phi_1^2/2\langle\phi_1^2\rangle_{av}} \qquad [44]$$

Thus, the phase distribution is the product of two independent functions. The function $h(x_0)$ represents the shape of the sample (it is the spin density function). We recall that the length of a chord at a distance of x_0 from the center of a circle of radius r is given using the Pythagorean theorem by $2(r^2 - x_0^2)^{1/2}$, and we define

$$h(x_0) = \begin{cases} \dfrac{2}{\pi r^2}(r^2 - x_0^2)^{1/2} & |x_0| \le r \\ 0 & |x_0| > r \end{cases} \qquad [45]$$

$h(x_0)$ describes the distribution of chords of a circle, a semi-ellipse, and is zero for a position outside the sample, and the normalization factor, $1/\pi r^2$, has been included as we require

$$\int_{-\infty}^{\infty} h(x_0) = \int_{-r}^{r} h(x_0) = 1 \qquad [46]$$

Thus,

$$\begin{aligned} S(2\tau) &= S(2\tau)_{g=0} \int_{-\infty}^{\infty} P(\phi)\cos\phi \, d\phi \\ &= S(2\tau)_{g=0} \int_{-\infty}^{\infty} g(\phi_1)\, d\phi_1 \int_{-\infty}^{\infty} h(x_0) \\ &\quad \times \cos(\phi_1 + \gamma g(2\tau - t)x_0)\, dx_0 \end{aligned} \qquad [47]$$

We first consider the inner integral in Eq. [47],

$$\begin{aligned} &\int_{-\infty}^{\infty} h(x_0)\cos(\phi_1 + \gamma g(2\tau - t)x_0)\, dx_0 \\ &\quad = \cos\phi_1 \int_{-\infty}^{\infty} h(x_0)\cos(\gamma g(2\tau - t)x_0)\, dx_0 \\ &\quad\quad - \sin\phi_1 \int_{-\infty}^{\infty} h(x_0)\sin(\gamma g(2\tau - t)x_0)\, dx_0 \end{aligned} \qquad [48]$$

where we used the trigonometric identity

$$\cos(A + B) = \cos A \cos B - \sin A \sin B.$$

Now the second integral in Eq. [48] is an odd function of x_0, and so equals 0. Thus, Eq. [47] becomes

$$\begin{aligned} S(2\tau) &= S(2\tau)_{g=0} \int_{-\infty}^{\infty} g(\phi_1)\cos\phi_1 \, d\phi_1 \\ &\quad \times \int_{-\infty}^{\infty} h(x_0)\cos(\gamma g(2\tau - t)x_0)\, dx_0. \end{aligned} \qquad [49]$$

We first consider the integral over x_0 in Eq. [49],

$$\begin{aligned} &\int_{-\infty}^{\infty} h(x_0)\cos(\gamma g(2\tau - t)x_0)\, dx_0 \\ &\quad = \frac{2}{\pi r^2} \int_{-r}^{r} (r^2 - x_0^2)^{1/2} \cos(\gamma g(2\tau - t)x_0)\, dx_0 \end{aligned} \qquad [50]$$

and set $x_0 = rt$, and so $dx_0 = r\,dt$ and thus

$$= \frac{2}{\pi} \int_{-1}^{1} (1 - t^2)^{1/2} \cos(\gamma g(2\tau - t)rt)\, dt \qquad [51]$$

We use the integral representation of the first-order Bessel function (e.g., Eq. [8], p. 962 in Ref. *104*)

$$J_\nu(x) = \frac{\left(\frac{z}{2}\right)^\nu}{\Gamma\left(\nu + \frac{1}{2}\right)\Gamma\left(\frac{1}{2}\right)} \times \int_{-1}^{1} (1 - t^2)^{\nu - 1/2} \cos(zt) \qquad \left[\mathrm{Re}\,\nu > -\frac{1}{2}\right] \quad [52]$$

where Γ is the gamma function (*104*) and in our case $\nu = 1$ and $z = \gamma g(2\tau - t)r$, $\Gamma(1/2) = \sqrt{\pi}$, $\Gamma(3/2) = \sqrt{\pi}/2$, and so Eq. [52] becomes

$$J_1(x) = \frac{\frac{z}{2}}{\Gamma\left(\frac{3}{2}\right)\Gamma\left(\frac{1}{2}\right)} \int_{-1}^{1} (1 - t^2)^{1/2} \cos(zt) = \frac{z}{\pi} \int_{-1}^{1} (1 - t^2)^{1/2} \cos(zt) \quad [53]$$

Using Eq. [53], Eq. [50] becomes

$$\frac{2}{\pi} \int_{-1}^{1} (1 - t^2)^{1/2} \cos(\gamma g(2\tau - t)rt)\, dt = \frac{2}{\gamma g(2\tau - t)r} \left[\frac{\gamma g(2\tau - t)r}{\pi} \int_{-1}^{1} (1 - t^2)^{1/2} \cos(\gamma g(2\tau - t)rt)\, dt \right] = \frac{2J_1(\gamma g(2\tau - t)r)}{\gamma g(2\tau - t)r} \quad [54]$$

We now consider the integral over ϕ_1 in Eq. [49],

$$\int_{-\infty}^{\infty} g(\phi_1) \cos\phi_1\, d\phi_1 = \frac{1}{\sqrt{2\pi\langle\phi_1^2\rangle_{av}}} \int_{-\infty}^{\infty} e^{-\phi_1^2/2\langle\phi_1^2\rangle_{av}} \cos\phi_1\, d\phi_1 = \frac{2}{\sqrt{2\pi\langle\phi_1^2\rangle_{av}}} \int_{0}^{\infty} e^{-\phi_1^2/2\langle\phi_1^2\rangle_{av}} \cos\phi_1\, d\phi_1 \quad [55]$$

By noting the standard integral (e.g., 3.896.4 in Ref. *104*)

$$\int_0^\infty e^{-\beta x^2} \cos(bx)\, dx = \frac{1}{2}\sqrt{\frac{\pi}{\beta}} \exp\left(-\frac{b^2}{4\beta}\right) \qquad [\mathrm{Re}\,\beta > 0] \quad [56]$$

where in the present case $\beta = 1/(2\langle\phi_1^2\rangle_{av})$ and $b = 1$, and so continuing with Eq. [55], we get

$$\int_{-\infty}^{\infty} g(\phi_1)\cos\phi_1\, d\phi_1 = \frac{2}{\sqrt{2\pi\langle\phi_1^2\rangle_{av}}} \frac{1}{2}\sqrt{\pi\langle\phi_1^2\rangle_{av}} \exp\left(-\frac{2\langle\phi_1^2\rangle_{av}}{4}\right) = \exp\left(-\frac{\langle\phi_1^2\rangle_{av}}{2}\right) \quad [57]$$

Using Eq. [54] and [57], we finally obtain the solution to Eq. [47] as (*28*, *103*)

$$S(2\tau) = S(2\tau)_{g=0} \int_{-\infty}^{\infty} g(\phi_1)\, d\phi_1 \int_{-\infty}^{\infty} h(x_0) \times \cos(\phi_1 + \gamma g(2\tau - t)x_0)\, dx_0 = \exp\left(-\frac{\langle\phi_1^2\rangle_{av}}{2}\right) \frac{2J_1(\gamma g(2\tau - t)r)}{\gamma g(2\tau - t)r} \quad [58]$$

(n.b., Refs. *28* and *103* contain misprints; the 2 has been omitted in the numerator).

For the purposes of gradient calibration, however, it is important to keep in mind that the exponential term in Eq. [58] is a constant (it is the attenuation factor due to diffusion and does not affect the echo shape, only its initial amplitude) and to consider the Fourier transform of $J_1(\gamma g(2\tau - t)r)/\gamma g(2\tau - t)r$ and thereby obtain the frequency spectrum,

$$S(\omega) = \int_{-\infty}^{\infty} \frac{J_1(\gamma g(2\tau - t)r)}{\gamma g(2\tau - t)r} e^{-i\omega t}\, dt \quad [59]$$

We set $a = \gamma gr$, $x = a(2\tau - t)$, $t = 2\tau - x/a$, and $dt = -dx/a$, and so Eq. [59] becomes

$$S(\omega) = -\int_{-\infty}^{\infty} \frac{J_1(x)}{ax} e^{-i\omega(2\tau - \frac{x}{a})}\, dx = -\frac{e^{-i\omega 2\tau}}{a} \int_{-\infty}^{\infty} \frac{J_1(x)}{x} e^{i\omega\frac{x}{a}}\, dx = -\frac{e^{-i\omega 2\tau}}{a} F(\omega) \quad [60]$$

We set $k = \dfrac{\omega}{a}$ and consider the integral

$$F(\omega) = \int_{-\infty}^{\infty} \frac{J_1(x)}{x} e^{ikx}\, dx \qquad [61]$$

which, by recalling that $e^{ikx} = \cos(kx) + i\sin(kx)$, becomes

$$F(\omega) = \int_{-\infty}^{\infty} \frac{J_1(x)}{x} \cos(kx)\, dx + i\int_{-\infty}^{\infty} \frac{J_1(x)}{x} \sin(kx)\, dx \qquad [62]$$

We note that the first integrand is even and the second integrand is odd and therefore goes to zero, and so Eq. [62] becomes

$$F(\omega) = 2\int_{0}^{\infty} \frac{J_1(x)}{x} \cos(kx)\, dx \qquad [63]$$

Next, we note the standard integral (e.g., 6.693.2 in Ref. *104*)

$$\int_0^{\infty} \frac{J_\nu(\alpha x)}{x} \cos \beta x\, dx = \begin{cases} \dfrac{1}{\nu}\cos\left(\arcsin\dfrac{\beta}{\alpha}\right) & [\beta \le \alpha] \\ \dfrac{\alpha^\nu \cos\dfrac{\nu\pi}{2}}{\nu\left(\beta + \sqrt{\beta^2 - \alpha^2}\right)^\nu} & [\beta \ge \alpha] \end{cases} \quad [\mathrm{Re}\,\nu > 0] \qquad [64]$$

in the present case $\nu = 1$, $\alpha = 1$, and $\beta = k$. Thus, Eq. [59] becomes

$$S(\omega) = -\frac{e^{-i\omega 2\tau}}{\gamma g r} \cos\left(\arcsin\left(\frac{\omega}{\gamma g r}\right)\right) \quad [|\omega| \le \gamma g r] \qquad [65]$$

and equals 0 otherwise.

As an aside, we consider Eq. [58] when $t = 2\tau$. We can calculate $\langle \phi^2 \rangle_{av}$ using the methods described previously (i.e., see Part 1, The GPD Approximation, especially Eq. [59], and set the limits of integration in accordance with the spin-echo sequence with a constant gradient) to be

$$\langle \phi^2 \rangle_{av} = \gamma^2 g^2 \frac{4}{3} \tau^3 D \qquad [66]$$

and noting

$$\lim_{t \to 2\tau} \left(\frac{2J_1(\gamma g(2\tau - t)r)}{\gamma g(2\tau - t)r} \right) = 1 \qquad [67]$$

and so Eq. [58] becomes

$$S(2\tau) = \exp\left(-\frac{\gamma^2 g^2 \frac{4}{3}\tau^3 D}{2} \right) \times \lim_{t \to 2\tau} \left(\frac{2J_1(\gamma g(2\tau - t)r)}{\gamma g(2\tau - t)r} \right) = \exp\left(-\gamma^2 g^2 \frac{2}{3} \tau^3 D \right) \qquad [68]$$

as expected for the Hahn spin-echo sequence excluding the effects of spin–spin relaxation.

Case 2: Gradient Directed along the Cylinder. Nowadays, we are more likely to be using a superconducting magnet with the gradient direction along the z axis, i.e., $g = g_z$. In this case, we define

$$h(z_0) = \begin{cases} \dfrac{1}{l} & |z_0| \le l \\ 0 & |z_0| > l \end{cases} \qquad [69]$$

(i.e., $1/l$ is the normalization factor) and, performing the same procedure as in the previous subsection, we have

$$S(2\tau) = S(2\tau)_{g=0} \int_{-\infty}^{\infty} g(\phi_1) \cos\phi_1\, d\phi_1 \times \int_{-\infty}^{\infty} h(z_0) \cos(\gamma g(2\tau - t) z_0)\, dz_0 \qquad [70]$$

We first consider the integral over z_0 in Eq. [70],

$$\int_{-\infty}^{\infty} h(z_0) \cos(\gamma g(2\tau - t) z_0)\, dz_0 = \frac{1}{l}\int_0^{l} \cos(\gamma g(2\tau - t) z_0)\, dz_0 = \frac{\sin(\gamma g(2\tau - t) l)}{\gamma g(2\tau - t) l} \qquad [71]$$

The integral in Eq. [70] over ϕ_1 is given by Eq. [57], and so Eq. [70] becomes

$$S(2\tau) = \exp\left(-\frac{\langle\phi_1^2\rangle_{av}}{2}\right)\frac{\sin(\gamma g(2\tau - t)l)}{\gamma g(2\tau - t)l}$$
$$= \exp\left(-\frac{\langle\phi_1^2\rangle_{av}}{2}\right)\mathrm{sinc}(\gamma g(2\tau - t)l) \quad [72]$$

Of course, if we substitute $t = 2\tau$, we obtain the same answer as in Eq. [68]. However, what is more interesting is to keep in mind that the first term in Eq. [72] is a constant and to consider the Fourier transform $\mathrm{sinc}(\gamma g(2\tau - t)l)$, and thereby obtain the frequency spectrum

$$S(\omega) = \int_{-\infty}^{\infty}\frac{\sin(\gamma g(2\tau - t)l)}{\gamma g(2\tau - t)l}e^{-i\omega t}\,dt \quad [73]$$

We set $a = \gamma gl$, $x = a(2\tau - t)$, $t = 2\tau - x/a$, and $dt = -dx/a$, and so Eq. [73] becomes

$$S(\omega) = -\int_{-\infty}^{\infty}\frac{\sin x}{ax}e^{-i\omega(2\tau - \frac{x}{a})}\,dx$$
$$= -\frac{e^{-i2\tau\omega}}{a}\int_{-\infty}^{\infty}\frac{\sin x}{x}e^{ikx}\,dx$$
$$= -\frac{e^{-i2\tau\omega}}{a}F(\omega) \quad [74]$$

where $k = \dfrac{\omega}{a}$. We now consider the integral

$$F(\omega) = \int_{-\infty}^{\infty}\frac{\sin x}{x}e^{ikx}\,dx \quad [75]$$

Noting that $e^{ikx} = \cos(kx) + i\sin(kx)$, we have

$$F(\omega) = F_1(\omega) + iF_2(\omega) \quad [76]$$

where

$$F_1(\omega) = \int_{-\infty}^{\infty}\frac{\sin x\cos x}{x}\,dx = 2\int_0^{\infty}\frac{\sin x\cos x}{x}\,dx \quad [77]$$

(n.b., the integrand is even) and

$$F_2(\omega) = \int_{-\infty}^{\infty}\frac{\sin x\sin kx}{x}\,dx = 0 \quad [78]$$

because the integrand is odd. Next, we note the identity

$$\sin x\cos(kx) = \frac{1}{2}[\sin(x[1 - k]) + \sin(x[1 + k])] \quad [79]$$

and so Eq. [77] becomes

$$F_1(\omega) = \int_0^{\infty}\frac{\sin([1 - k]x)}{x}\,dx + \int_0^{\infty}\frac{\sin([1 + k]x)}{x}\,dx \quad [80]$$

Finally, we note the standard integral (e.g., see Eq. 2.5.3.12 in Ref. *105*)

$$\int_0^{\infty}\frac{\sin bx}{x}\,dx = \frac{\pi}{2}\mathrm{sgn}\,b \quad [81]$$

(i.e., $\mathrm{sgn}\,x = +1$ for $x > 0$; $\mathrm{sgn}\,x = -1$ for $x < 0$). Thus,

$$F(\omega) = \frac{\pi}{2}[\mathrm{sgn}(1 - k) + \mathrm{sgn}(1 + k)]$$
$$= \frac{\pi}{2}\left[\mathrm{sgn}\left(1 - \frac{\omega}{\gamma gl}\right) + \mathrm{sgn}\left(1 + \frac{\omega}{\gamma gl}\right)\right]$$
$$= \frac{\pi}{2}[\mathrm{sgn}(\gamma gl - \omega) + \mathrm{sgn}(\gamma gl + \omega)] \quad [82]$$

and so, substituting back into Eq. [74], we finally get

$$S(\omega) = -\frac{e^{-i2\tau\omega}}{\gamma gl}\frac{\pi}{2}[\mathrm{sgn}(\gamma gl - \omega) + \mathrm{sgn}(\gamma gl + \omega)] \quad [83]$$

Now, the bracketed term in Eq. [83] will only be nonzero when $|\omega| \le \gamma gl$ as expected for the transform of a sinc function. In fact, even without doing such cumbersome analysis, it is easy to see the shape of Eq. [83] from simple reasoning with the Larmor equation. For example, if we arbitrarily take the magnetic field at one end of the cylinder to be B_0, and so the lowest resonance frequency will be γB_0, then at a distance l in the direction of the gradient the magnetic field must be $B_0 + gl$, and thus the highest resonance frequency must be $\gamma(B_0 + gl)$. Since the number of spins is constant along the cylinder axis, the absolute value of the Fourier transform of the signal

must be rectangular with a line width $\Delta\nu$ (Hz), given by

$$\Delta\nu = \frac{\gamma g l}{2\pi} \qquad [84]$$

Performing Echo Shape Analysis and One-Dimensional Imaging. If a constant gradient is used throughout the echo sequence, the rf pulse must have sufficient power to excite the gradient broadened spectrum. Roughly, the strength of the rf pulse must be larger than the $g \times d_s$, where d_s is the characteristic distance of the sample in the direction of the gradient. As the rf power becomes insufficient, the measured value of g will not increase in proportion to I. A better solution is to use the pulse sequence given in Fig. 19. Although this removes the constraint on the rf pulse power, even modest gradients require large receiver bandwidths (see Eq. [84]) to acquire the signal. Furthermore, as the gradient is increased, more scans will need to be averaged to obtain sufficient signal-to-noise. An example of the FIDs acquired for a gradient across the cylinder (i.e., g_x) and along the cylinder axis (i.e., g_z) is given in Fig. 19.

The gradients can then be calculated by analyzing the shape of the respective FIDs. For example, in the case of a gradient transverse to the cylinder axis, the gradient strength is determined from the zeros of the echo (Fig. 19) which correspond to the zeroes in $(J_1(\gamma g(2\tau - t)r))/\gamma g(2\tau - t)r$ (see Eq. [58], n.b., the only unknown is g). As pointed out by a number of workers (*106–110*), this method is prone to a number of systematic errors—for example, if the cylinder axis is not perfectly perpendicular to the gradient.

A partial solution to some of the shortcomings of this method is to analyze the Fourier-transformed spectrum instead of looking for the zeroes of the function. The Fourier transform of the gradient-broadened FID (i.e., a one-dimensional image) (Fig. 19) also provides the information in a more easily accessible form (*9*, *108*, *109*). The gradient strength can then be determined from the width of the gradient-broadened resonance (i.e., Eq. [83]). This method also allows some indication of the gradient linearity from the one-dimensional image. This method is still limited by the spectrometer bandwidth. Typically, this method is most useful in the case where the gradient is along the cylinder axis, since the shape of the image is ideally rectangular (Fig. 19). The FID is recorded in the presence of the gradient for a number of different applied currents, and then by plotting the width of the spectrum versus the current, the gradient strength can be calibrated (*9*). If the transmitter offset is placed at the resonance frequency of the sample (i.e., in the absence of the gradient), then, if the sample is correctly centered in the gradient, the gradient broadened spectrum will expand symmetrically around the transmitter offset as the gradient strength is increased. This method requires that the length of the sample containing cell be known accurately, and the final calibration will have an error of $< 5\%$. Two virtues of this method are that the calibration can be performed without knowledge of the sample diffusion coefficient, and as long as the dimensions of the container holding the sample are not temperature sensitive (or at least very small, like glass), it can be used to cross-check that the gradient strength is not temperature dependent. However, this method has a limited range of application since for anything more than modest gradients, the gradient-broadened spectrum is larger than the maximum spectrometer bandwidth (see Eq. [84]).

Intentional Gradient Pulse Mismatch

Hrovat and Wade (*31*, *34*, *111*) suggested using the time displacement of the echo maximum caused by the intentional mismatch of gradient pulses. Their procedure is based on the following idea:

$$t_{\text{echo}} = \frac{2\tau - g\varepsilon\cos(\alpha)}{g_0} \qquad [85]$$

and the attenuation with respect to the case where $g_0 = 0$ is given by

$$E = \frac{2J_1[\gamma Rq\varepsilon\sin(\alpha)]}{\gamma Rq\varepsilon\sin(\alpha)} \qquad [86]$$

which is a maximum as expected for $\varepsilon = 0$ (i.e., $E \to 1$ as $\varepsilon \to 0$; see Eq. [67] and making appropriate changes to the variables). The background gradient g_0 can be determined from the line shape of the spin-echoes, and then from Eqs. [85] and [86] g and α can be determined. From Eq. [85], it can be seen that the sensitivity of t_{echo} to ε increases as g_0 becomes smaller.

A Practical Calibration Procedure

If confronted with an uncalibrated coil, a realistic calibration procedure is to first perform a theoretical calculation of what gradient the coil should produce for a given current (of course, with commercial equipment; an estimate of the gradient strength will be provided as part of the specifications). A one-dimensional image should then be used for experimental verification. Finally, if a suitable reference compound exists, this should be used for fine-tuning the calibration. The other methods mentioned above can also be used, but this procedure is the simplest.

For completeness, we note that if the diffusion probe is equipped with more than one gradient, it is proposed that the measured diffusion anisotropy in isotropic media can be used as a basis for calibrating and aligning magnetic field gradients (*112*).

PERFORMING AND ANALYZING PFG EXPERIMENTS

The PFG experiment is performed by varying one of the experimental variables (i.e., δ, Δ, or $\mathbf{g}$) while τ is generally kept constant so that relaxation may be factored out (see Eq. [2]). However, which one of δ, Δ, or $\mathbf{g}$ is varied will depend on the type of information that we require and the system that we are studying. Of course, we must first calibrate the gradient strength as described in Gradient Calibration, and we must also determine the minimum time required for the eddy current effects to dissipate for the maximum gradient strength we intend to use (see Eddy Currents and Perturbation of B_0). Assuming that the delay required is not so large compared to the relaxation time of the species in question that it would cause the value of Δ to be too short, it is preferable to use the simple Stejskal and Tanner sequence for two reasons: (a) it is a simpler sequence with trivial phase-cycling requirements (cw the STE sequence), and (b) there are no complications from cross-relaxation effects. If the resonance is *J*-coupled, the value of τ used should be chosen according to the coupling constant (see *J* Modulation). If the sample contains internal gradients, it is necessary to use one of the sequences presented in Internal Gradients. A rough guide of the applicability of the sequences, together with some examples of their application, is given in Table 9. If eddy currents are a problem, the LED, bipolar gradient, or other sequences outlined in Eddy Currents and Perturbation of B_0 may be used, and if the observed spin system is suitable, multiple quantum PFG sequences may also be used. Many of the sample-related problems are alleviated through the use of a short susceptibility-matched sample as shown in Fig. 12.

There is basically no difference apart from the matter of NMR sensitivity whether one works with heteronuclei or protons. A negative aspect, however, is that because of their lower γ, diffusion measurements using heteronuclei generally require greater gradient strengths; but conversely, they are less susceptible to the effects of eddy currents. As noted in *J* Modulation, it is generally inadvisable to apply broadband decoupling during the PFG sequence, and generally this should be applied only during the recycle delay to obtain NOE enhancement and acquisition to re-

Table 9 PFG Sequences and Applicability with Some Literature Examples

Sequence	Necessary Conditions	Typical Samples	Examples
Stejskal and Tanner	Best when $T_2 \gtrsim \tau$	Liquids, small molecules	Glycine (*125*), Na^+ (*126*)
Stimulated echo	Best when $T_1 > T_2$	Proteins, polymers	Parvalbumin (*127*)
LED	General	As for S & T or STE but with reduced eddy current problems	Myosin light chain 2 (*128*), various proteins (*129*)
Background gradients		Samples with large internal gradients	Hydrides (*91*), gels containing iron particles (*77*)
Multiple quantum	Static dipolar, quadrupolar couplings, scalar couplings	Those that meet the necessary conditions	Phosphorus acid (*94*), benzene in liquid crystal (*97*) $^7Li^+$ in ordered DNA (*99*)

Further examples can be found elsewhere (e.g., Refs. *7* and *124*).

move the couplings. Signal-to-noise problems with heteronuclei may also be alleviated by using inverse detection and the like (see Multiple Quantum and Heteronuclear Experiments).

Often solvent suppression will be a problem, especially for low values of q, many possibilities exist for removing the solvent signal, especially those that can be placed before the PFG diffusion sequence. Examples include presaturation or water-PRESS (*113*) and others (*114*). As the value of q increases, the solvent signal is almost never a problem, since its intensity is reduced much faster than that of the (more slowly moving) species of interest by the PFG attenuation. This is, in fact, the basis of another well-known method of water suppression, DRYCLEAN (*115*).

Typically, to obtain accurate diffusion coefficients of freely diffusing samples, it is desirable to record the echo attenuation over at least two orders of magnitude, although if the signal-to-noise ratio is very good, it is possible to determine the diffusion coefficient from a signal attenuation of only 1%. However, measuring to high degrees of attenuation allows the effects of restricted diffusion, if present, to be visualized. It might seem advantageous to use absolute value (also referred to as power or magnitude) spectra to overcome eddy current–induced phase instability and the like. This is true only in the case of first-order spectra or overlapped spectra (*4*). It is preferable to correct the data in phase-sensitive mode since, apart from the better spectral resolution, phase changes related to the gradient parameters are good indicators of eddy current effects and their absence provides some confidence that the data are artifact free.

Because of the γ dependence of the attenuation, it is normally preferable to use high γ nuclei as the probe nuclei. To set cogent values for Δ, δ, and g in the experiment, it is worthwhile (assuming the simplest case of a monodisperse single species) to simulate the experiment using Eq. [2] with an approximate value for the diffusion coefficient.

A very obvious way to analyze the data, especially if a rough-and-ready analysis is acceptable, is simply to plot $\ln(E)$ versus $\gamma^2 g^2 \delta^2 (\Delta - \delta/3)$, in which case the diffusion coefficient can be obtained from the slope (i.e., $-D$). However, this approach gives unequal weighting to the noise, particularly as the signal approaches zero. For this reason, when higher accuracy is called for, it is better to use nonlinear regression of the relevant attenuation equation onto the experimental data. We note that von Meerwall and Ferguson wrote a specialized computer program for analyzing attenuation data with respect to a number of pertinent models (*116*).

CONCLUDING REMARKS

This article does not claim to be exhaustive in its coverage of pulse sequences for measuring diffusion and many other sequences exist [e.g., (*7*, *117*)], nor were special methods for measuring diffusion in solids considered (*5*). In passing, we note that in particular, the review by Stilbs (*4*) also considered some experimental and technical aspects. In the present article, we have introduced some of the technical aspects related to performing PFG diffusion measurements, and also to their analysis for simple systems. The single most important conclusion to draw from this article is that the reliability of the diffusion measurements depends on the spectrometer and gradient system being well characterized and calibrated.

APPENDIX

Maple Worksheet for the Stejskal and Tanner Equation, Including Gradient Pulses with Infinitely Fast Rise Times and Long Eddy Currents

Reset the system

```
> restart;
```

Define the integral used in determining F

```
> F := (G, ti) → int (G, t = ti..tf);
```

Define the time intervals and the relevant value of g for each integral. Also calculate the value of F for each interval remembering that it contains the contribution from all of the intervals from the start of the pulse sequence.

```
> l1 := 0;
> g1 := 0;
> F1 := F(g1, l1);

> l2 := t1;
> g2 := g;
> F2 := subs (tf = l2, F1) + F(g2, l2);

> l3 := t1 + delta;
> g3 := g*exp(- k*(t- l3));
> F3 := subs(tf = l3, F2) + F(g3, l3);
```

```
> l4 := t1 + Delta;
> g4 := g;
> F4 := subs(tf = l4, F3) + F(g4, l4);

> l5 := t1 + Delta + delta;
> g5 := g*exp(- k*(t- l5));
> F5 := subs(tf = l5, F4) + F(g5, l5);

> l6 := 2*tau;
```

Define the function "f" (= F(tau))

```
> f := subs(tf = tau, F3);
```

Define the integral of F between tau and 2*tau

```
> FINT := int(F3, tf = tau..l4) +
int(F4, tf = l4..l5) + int(F5, tf =
l5..l6);
```

Define the integral of F^2 between 0 and 2*tau

```
>FSQINT := int(F1^2, tf = l1..l2) +
int(F2^2, tf = l2..l3) + int(F3^2, tf =
l3..l4) + int(F4^2, tf = l4..l5) +
int(F5^2, tf = l5..l6);
```

Define the function to give the echo attenuation and simplify the result.

```
> ln(E) := simplify(- gamma^2*D*
(FSQINT- 4*f*FINT + 4*f^2*tau));
```

ACKNOWLEDGMENTS

Dr. Alexander V. Barzykin, Professor Paul T. Callaghan, and Dr. Sergey D. Traytak are thanked for useful suggestions. Dr. Kikuko Hayamizu is thanked for critically reading the manuscript. The reviewers are thanked for their detailed comments.

REFERENCES

1. W. S. Price, "Pulsed Field Gradient Nuclear Magnetic Resonance as a Tool for Studying Translational Diffusion: Part 1. Basic Theory," *Concepts Magn. Reson.*, **1997,** *9*, 299–336.
2. P. T. Callaghan, *Principles of Nuclear Magnetic Resonance Microscopy*, Clarendon, Oxford, 1991.
3. P. T. Callaghan, C. M. Trotter, and K. W. Jolley, "A Pulsed Field Gradient System for a Fourier Transform Spectrometer," *J. Magn. Reson.*, **1980,** *37*, 247–259.
4. P. Stilbs, "Fourier Transform Pulsed-Gradient Spin-Echo Studies of Molecular Diffusion," *Progr. NMR Spectrosc.*, **1987,** *19*, 1–45.
5. J. Kärger, H. Pfeifer, and W. Heink, "Principles and Applications of Self-diffusion measurements by Nuclear Magnetic Resonance," *Adv. Magn. Reson.*, **1988,** *12*, 1–89.
6. W. S. Price, W.-T. Chang, W.-M. Kwok, and L.-P. Hwang, "Design and Construction of a Pulsed Field-Gradient NMR Probe for a High-Field Superconducting Magnet," *J. Chin. Chem. Soc. (Taipei)*, **1994,** *41*, 119–127.
7. W. S. Price, "Gradient NMR," in *Annual Reports on NMR Spectroscopy*, Vol. 32, G. A. Webb, Ed., Academic, London, 1996, pp. 51–142.
8. W. S. Price, "NMR Imaging," in *Annual Reports on NMR Spectroscopy*, Vol. 35, G. A. Webb, Ed., Academic, London, 1998, pp. 139–216.
9. W. S. Price, "An NMR Study of Diffusion, Viscosity, and Transport of Small Molecules in Human Erythrocytes," Ph.D. dissertation, University of Sydney, 1990.
10. W. R. Smythe, *Static and Dynamic Electricity*, McGraw-Hill, New York, 1939.
11. M. Abramowitz and I. A. Stegun, *Handbook of Mathematical Functions*, Dover, New York, 1970.
12. P. Mansfield and B. Chapman, "Active Magnetic Screening of Gradient Coils in NMR Imaging," *J. Magn. Reson.*, **1986,** *66*, 573–576.
13. P. Mansfield and B. Chapman, "Active Magnetic Screening of Coils for Static and Time-Dependent Magnetic Field Generation," *J. Phys.*, **1986,** *E19*, 540–545.
14. R. Turner, "A Target Field Approach to Optimal Coil Design," *J. Phys.*, **1986,** *D19*, L147–L151.
15. R. Turner and R. M. Bowley, "Passive Screening of Switched Magnetic Field Gradients," *J. Phys.*, **1986,** *E19*, 876–879.
16. J. W. Carlson, K. A. Derby, K. C. Hawryszko, and M. Weideman, "Design and Evaluation of Shielded Gradient Coils," *Magn. Reson. Med.*, **1992,** *26*, 191–206.
17. M. Burl and I. R. Young, "Eddy Currents and Their Control," in *Encyclopedia of Nuclear Magnetic Resonance*, Vol. 3, D. M. Grant and R. K. Harris, Eds., Wiley, New York, 1996, pp. 1841–1846.
18. A. Jasinski, T. Jakubowski, R. Rydzy, P. Morris, I. C. P. Smith, P. Kozlowski, and J. K. Saunders, "Shielded Gradient Coils and Radio Frequency Probes for High-Resolution Imaging of Rat Brains," *Magn. Reson. Med.*, **1992,** *24*, 29–41.
19. R. E. Hurd, A. Deese, M. O'Neil, S. Sukumar, and P. C. M. Van Zijl, "Impact of Differential Linearity in Gradient-Enhanced NMR," *J. Magn. Reson.*, **1996,** *A119*, 285–288.
20. B. Håkansson, B. Jönsson, P. Linse, and O. Söderman, "The Influence of a Nonconstant Magnetic-Field Gradient on PFG NMR Diffusion Experiments: A Brownian-Dynamics Computer Simulation Study," *J. Magn. Reson.*, **1997,** *124*, 343–351.
21. P. T. Callaghan, "PGSE–MASSEY, a Sequence for Overcoming Phase Instability in Very-High-Gradient Spin-Echo NMR," *J. Magn. Reson.*, **1990,** *88*, 493–500.

22. R. M. Boerner and W. S. Woodward, "A Computer-Controlled Bipolar Magnetic-Field-Gradient Driver for NMR Electrophoretic and Self-Diffusion Measurements," *J. Magn. Reson.*, **1994,** *A106*, 195–202.
23. N. K. Bär, J. Kärger, C. Krause, W. Schmitz, and G. Seiffert, "Pitfalls in PFG NMR Self-diffusion Measurements with Powder Samples," *J. Magn. Reson.*, **1995,** *A113*, 278–280.
24. M. Appel and G. Fleischer, "Investigation of the Chain Length Dependence of Self-diffusion of Poly(dimethyl siloxane) and Poly(ethylene oxide) in the Melt with Pulsed Field Gradient NMR," *Macromolecules*, **1993,** *26*, 5520–5525.
25. W. Heink, J. Kärger, G. Seiffert, G. Fleischer, and J. Rauchfuss, "PFG NMR Self-diffusion Measurements with Large Field Gradients," *J. Magn. Reson.*, **1995,** *A114*, 101–104.
26. P. T. Gallaghan, K. W. Jolley, and C. M. Trotter, "Stable and Accurate Spin Echoes in Pulsed Gradient NMR," *J. Magn. Reson.*, **1980,** *39*, 525–527.
27. H. Y. Carr and E. M. Purcell, "Effects of Diffusion on Free Precession in Nuclear Magnetic Resonance Experiments," *Phys. Rev.*, **1954,** *94*, 630–638.
28. D. C. Douglass and D. W. McCall, "Diffusion in Paraffin Hydrocarbons," *J. Chem. Phys.*, **1958,** *62*, 1102–1107.
29. T. R. Saarinen and C. S. Johnson, Jr., "Imaging of Transient Magnetization Gratings in NMR: Analogies with Laser-Induced Gratings and Applications to Diffusion and Flow," *J. Magn. Reson.*, **1988,** *78*, 257–270.
30. W. S. Price and P. W. Kuchel, "Effect of Nonrectangular Field Gradient Pulses in the Stejskal and Tanner (Diffusion) Pulse Sequence," *J. Magn. Reson.*, **1991,** *94*, 133–139.
31. M. I. Hrovat and C. G. Wade, "NMR Pulsed-Gradient Diffusion Measurements. I. Spin-Echo Stability and Gradient Calibration," *J. Magn. Reson.*, **1981,** *44*, 62–75.
32. X. X. Zhu and P. M. Macdonald, "Empirical Compensation Function for Eddy Current Effects in Pulsed Field Gradient Nuclear Magnetic Resonance Experiments," *Solid State Nucl. Magn. Reson.*, **1995,** *4*, 217–227.
33. E. von Meerwall and M. Kamat, "Effect of Residual Field Gradients on Pulsed Gradient NMR Diffusion Measurements," *J. Magn. Reson.*, **1989,** *83*, 309–323.
34. M. I. Hrovat and C. G. Wade, "NMR Pulsed Gradient Diffusion Measurements. II. Residual Gradients and Lineshape Distortions," *J. Magn. Reson.*, **1981,** *45*, 67–80.
35. Maple V, Rel. 4, Waterloo Maple, Waterloo, Ontario, Canada, 1996.
36. E. von Meerwall and R. D. Ferguson, "Interpreting Pulsed-Gradient Spin-Echo Diffusion Experiments with Permeable Membranes," *J. Chem. Phys.*, **1981,** *74*, 6956–6959.
37. J. J. Van Vaals and A. H. Bergman, "Optimization of Eddy-Current Compensation," *J. Magn. Reson.*, **1990,** *90*, 52–70.
38. P. D. Majors, J. L. Blackley, S. A. Altobelli, A. Caprihan, and E. Fukushima, "Eddy Current Compensation by Direct Field Detection and Digital Gradient Modification," *J. Magn. Reson.*, **1990,** *87*, 548–553.
39. P. Jehenson, M. Westphal, and N. Schuff, "Analytical Method for the Compensation of Eddy-Current Effects Induced by Pulsed Magnetic Field Gradients in NMR Systems," *J. Magn. Reson.*, **1990,** *90*, 264–278.
40. M. A. Morich, D. A. Lampman, W. R. Dannels, and F. T. D. Goldie, "Exact Temporal Eddy Current Compensation in Magnetic Resonance Imaging Systems," *IEEE Trans. Med. Imag.*, **1988,** *7*, 247–254.
41. J. Jehenson and A. Syrota, "Correction of Distortions Due to the Pulsed Magnetic Field Gradient-Induced Shift in B_0 Field by Postprocessing," *Magn. Reson. Med.*, **1989,** *12*, 253–256.
42. S. Crozier, F. A. Beckey, C. D. Eccles, J. Field, and D. M. Doddrell, "Correction for the Effect of Induced B_0 Shifts in Localized Spectroscopy and Imaging by Direct Frequency Modulation," *J. Magn. Reson.*, **1994,** *B103*, 115–119.
43. L. Griffiths, R. Horton, and T. Cosgrove, "NMR Diffusion Measurements Using Refocused Three-Pulse Stimulated Echoes," *J. Magn. Reson.*, **1990,** *90*, 254–263.
44. S. J. Gibbs and C. S. Johnson, Jr., "A PFG NMR Experiment for Accurate Diffusion and Flow Studies in the Presence of Eddy Currents," *J. Magn. Reson.*, **1991,** *93*, 395–402.
45. J. E. Tanner, "Use of the Stimulated Echo in NMR Diffusion Studies," *J. Chem. Phys.*, **1970,** *52*, 2523–2526.
46. D. Wu, A. Chen, and C. S. Johnson, Jr., "An Improved Diffusion-Ordered Spectroscopy Experiment Incorporating Bipolar-Gradient Pulses," *J. Magn. Reson.*, **1995,** *A115*, 260–264.
47. D. Burstein, "Stimulated Echoes: Description, Applications, Practical Hints," *Concepts Magn. Reson.*, **1996,** *8*, 269–278.
48. G. Wider, V. Dötsch, and K. Wüthrich, "Self-Compensating Pulsed Magnetic-Field Gradients for Short Recovery Times," *J. Magn. Reson.*, **1994,** *A108*, 255–258.
49. E. O. Stejsksal and J. E. Tanner, "Spin Diffusion Measurements: Spin Echoes in the Presence of a Time-Dependent Field Gradient," *J. Chem. Phys.*, **1965,** *42*, 288–292.
50. B. Gross and R. Kosfeld, "Anwendung der Spin-Echo-Methode bei der Messung der Selbstdiffusion," *Messtechnik*, **1969,** *7/8*, 171–177.

51. M. R. Merrill, "NMR Diffusion Measurements Using a Composite Gradient PGSE Sequence," *J. Magn. Reson.*, **1993,** *A103*, 223–225.
52. R. J. Ordridge and I. D. Cresshull, "The Correction of Transient B_0 Field Shifts following the Application of Pulsed Gradients by Phase Correction in the Time Domain," *J. Magn. Reson.*, **1986,** *69*, 151–155.
53. G. A. Morris, "Compensation of Instrumental Imperfections by Deconvolution Using an Internal Reference Signal," *J. Magn. Reson.*, **1988,** *80*, 547–552.
54. S. L. Talagala and I. J. Lowe, "Introduction to Magnetic Resonance Imaging," *Concepts Magn. Reson.*, **1991,** *3*, 145–159.
55. Y. Xia, "Contrast in NMR Imaging and Microscopy," *Concepts Magn. Reson.*, **1996,** *8*, 205–225.
56. X.-A. Mao and C.-H. Ye, "Understanding Radiation Damping in a Simple Way," *Concepts Magn. Reson.*, **1997,** *9*, 173–187.
57. G. N. Chmurny and D. I. Hoult, "The Ancient and Honourable Art of Shimming," *Concepts Magn. Reson.*, **1990,** *2*, 131–149.
58. D.-H. Wu, W. S. Woodward, and C. S. Johnson, Jr., "A Sample Spinner for Vibration-Sensitive Liquid-State Experiments with Application to Diffusion-Ordered 2D NMR," *J. Magn. Reson.*, **1993,** *A104*, 231–233.
59. A. L. Van Geet, "Calibration of the Methanol and Glycol Nuclear Magnetic Resonance Thermometers with a Static Thermistor Probe," *Anal. Chem.*, **1968,** *40*, 2227–2229.
60. A. L. Van Geet, "Calibration of Methanol Nuclear Magnetic Resonance Thermometer at Low Temperature," *Anal. Chem.* **1970,** *42*, 679–680.
61. D. S. Raiford, C. L. Fisk, and E. D. Becker, "Calibration of Methanol and Ethylene Glycol Nuclear Magnetic Resonance Thermometers," *Anal. Chem.*, **1979,** *51*, 2050–2051.
62. D.-J. Wang and J. S. Leigh, "Wireless Precision Piezoelectric Thermometer Using an RF Excitation-Detection Technique with an NMR probe," *J. Magn. Reson.*, **1994,** *105*, 25–30.
63. W. A. Bubb, K. Kirk, and P. W. Kuchel, "Ethylene Glycol as Thermometer for X-nucleus Spectroscopy in Biological Samples," *J. Magn. Reson.*, **1988,** *77*, 363–368.
64. A. Jerschow and N. Müller, "Suppression of Convection Artifacts in Stimulated-Echo Diffusion Experiments: Double-Stimulated-Echo Experiments," *J. Magn. Reson.*, **1997,** *125*, 372–375.
65. W. J. Goux, L. A. Verkruyse, and S. J. Salter, "The Impact of Rayleigh-Benard Convection on NMR Pulsed Field Gradient Diffusion Measurements," *J. Magn. Reson.*, **1990,** *88*, 609–614.
66. G. Arfken, *Mathematical Methods for Physicists*, Academic, New York, 1995.
67. Z. H. Endre, B. E. Chapman, and P. W. Kuchel, "Cell-Volume Dependence of ^{1}H Spin-Echo NMR Signals in Human Erythrocyte Suspensions: The Influence of *In Situ* Field Gradients," *Biochim. Biophys. Acta*, **1984,** *803*, 137–144.
68. P. W. Kuchel and B. T. Bulliman, "Pertubation of Homogeneous Magnetic Fields by Isolated Single and Confocal Spheroids: Implications for NMR Spectroscopy of Cells," *NMR Biomed.*, **1989,** *2*, 151–160.
69. J. Lian, D. S. Williams, and I. J. Lowe, "Magnetic Resonance Imaging of Diffusion in the Presence of Background Gradients and Imaging of Background Gradients," *J. Magn. Reson.*, **1994,** *A106*, 65–74.
70. W. D. Williams, E. F. W. Seymour, and R. M. Cotts, "A Pulsed-Gradient Multiple-Spin-Echo NMR Technique for Measuring Diffusion in the Presence of Background Magnetic Field Gradients," *J. Magn. Reson.*, **1978,** *31*, 271–282.
71. J. A. Glasel and K. H. Lee, "On the Interpretation of Water Nuclear Magnetic Resonance Relaxation Times in Heterogeneous Systems," *J. Am. Chem. Soc.*, **1974,** *96*, 970–978.
72. P. Gillis and S. H. Koenig, "Transverse Relaxation of Solvent Protons Induced by Magnetized Spheres: Application to Ferritin, Erythrocytes, and Magnetite," *Magn. Reson. Med.*, **1987,** *5*, 323–345.
73. S. Majumdar and J. C. Gore, "Studies of Diffusion in Random Fields Produced by Variations in Susceptibility," *J. Magn. Reson.*, **1988,** *78*, 41–55.
74. P. Bendel, "Spin-Echo Attenuation by Diffusion in Nonuniform Field Gradients," *J. Magn. Reson.*, **1990,** *86*, 509–515.
75. J. Zhong and J. C. Gore, "Studies of Restricted Diffusion in Heterogeneous Media Containing Variations in Susceptibility," *Magn. Reson. Med.*, **1991,** *19*, 276–284.
76. P. Le Doussal and P. N. Sen, "Decay of Nuclear Magnetization by Diffusion in a Parabolic Magnetic Field: An Exactly Solvable Model," *Phys. Rev.*, **1992,** *B46*, 3465–3485.
77. L. L. Latour, L. Li, and C. H. Sotak, "Improved PFG Stimulated-Echo Method for the Measurement of Diffusion in Inhomogeneous Fields," *J. Magn. Reson.*, **1993,** *B101*, 72–77.
78. T. M. De Swiet and P. N. Sen, "Decay of Nuclear Magnetization by Bounded Diffusion in a Constant Field Gradient," *J. Chem. Phys.*, **1994,** *100*, 5597–5604.
79. P. M. Joseph, "An Analytical Model for Diffusion of Spins in an Inhomogeneous Field Gradient," *J. Magn. Reson.*, **1994,** *B105*, 95–97.
80. I. Furo and H. Jóhannesson, "Accurate Anisotropic Water-Diffusion Measurements in Liquid Crystals," *J. Magn. Reson.*, **1996,** *A119*, 15–21.
81. J. S. Murday and R. M. Cotts, "Self-Diffusion in Molten Lithium," *Z. Naturforsch*, **1971,** *26a*, 85–93.

82. M. E. Moseley, J. Kucharczyk, H. S. Asgari, and D. Norman, "Anisotropy in Diffusion-Weighted MRI," *Magn. Reson. Med.*, **1991,** *19*, 321–326.
83. D. Le Bihan, "Molecular Diffusion, Tissue Microdynamics and Microstructure," *NMR Biomed.*, **1995,** *8*, 375–386.
84. J. D. Trudeau, W. Thomas Dixon, and J. Hawkins, "The Effect of Inhomogeneous Sample Susceptibility on Measured Diffusion Anisotropy Using MRI Imaging," *J. Magn. Reson.*, **1995,** *B108*, 22–30.
85. M. Neeman, J. P. Freyer, and L. O. Sillerud, "Pulsed-Gradient Spin-Echo Diffusion Studies in NMR Imaging: Effects of the Imaging Gradients on the Determination of the Diffusion Coefficients," *J. Magn. Reson.*, **1990,** *90*, 303–312.
86. D. Van Dusschoten, P. A. De Jager, and H. Van As, "Flexible PFG NMR Desensitized for Susceptibility Artifacts, Using the PFG Multiple-Spin-Echo Sequence," *J. Magn. Reson.*, **1995,** *A112*, 237–240.
87. J.-H. Zhong, R. P. Kennan, and J. C. Gore, "Effects of Susceptibility Variations on NMR Measurements of Diffusion," *J. Magn. Reson.*, **1991,** *95*, 267–280.
88. H. G. Sorland, B. Hafskjold, and O. Herstad, "A Stimulated-Echo Method for Diffusion Measurements in Heterogeneous Media Using Pulsed Field Gradients," *J. Magn. Reson.*, **1997,** *124*, 172–176.
89. A. V. Barzykin, W. S. Price, K. Hayamizu, and M. Tachiya, "Pulsed Field Gradient NMR of Diffusive Transport through a Spherical Interface into an External Medium Containing a Relaxation Agent," *J. Magn. Reson.*, **1995,** *A114*, 39–46.
90. K. J. Packer, C. Rees, and G. Tomlinson, "A Modification of the Pulsed Magnetic Field-Gradient Spin Echo Method of Studying Diffusion," *Mol. Phys.*, **1970,** *18*, 421–423.
91. R. F. Karlicek, Jr., and I. J. Lowe, "A Modified Pulsed Gradient Technique for Measuring Diffusion in the Presence of Large Background Gradients," *J. Magn. Reson.*, **1980,** *37*, 75–91.
92. R. M. Cotts, M. J. R. Hoch, T. Sun, and J. T. Markert, "Pulsed Field Gradient Stimulated Echo Methods for Improved NMR Diffusion Measurements in Heterogeneous Systems," *J. Magn. Reson.*, **1989,** *83*, 252–266.
93. L. J. C. Peschier, J. A. Bouwstra, J. De Bleyser, H. E. Junginger, and J. C. Leyte, "Cross-Relaxation Effects in Pulsed-Field-Gradient Stimulated-Echo Measurements on Water in a Macromolecular Matrix," *J. Magn. Reson.*, **1996,** *B110*, 150–157.
94. B. E. Chapman and P. W. Kuchel, "Sensitivity in Heteronuclear Multiple-Quantum Diffusion Experiments," *J. Magn. Reson.*, **1993,** *A102*, 105–109.
95. P. W. Kuchel and B. E. Chapman, "Heteronuclear Double-Quantum-Coherence Selection with Magnetic-Field Gradients in Diffusion Experiments," *J. Magn. Reson.*, **1993,** *A101*, 53–59.
96. J. F. Martin, L. S. Selwyn, R. R. Vold, and R. L. Vold, "The Determination of Translational Diffusion Constants in Liquid Crystals from Pulsed Field Gradient Double Quantum Spin Echo Decays," *J. Chem. Phys.*, **1982,** *76*, 2632–2634.
97. D. Zax and A. Pines, "Study of Anisotropic Diffusion of Oriented Molecules by Multiple Quantum Spin Echoes," *J. Chem. Phys.*, **1983,** *78*, 6333–6334.
98. L. E. Kay and J. H. Prestegard, "An Application of Pulse-Gradient Double Quantum Spin Echoes to Diffusional Measurements on Molecules with Scalar-Coupled Spins," *J. Magn. Reson.*, **1986,** *67*, 103–113.
99. L. van Dam, B. Andreasson, and L. Nordenskiöld, "Multiple-Quantum Pulsed Gradient NMR Diffusion Experiments on Quadrupolar ($I > 1/2$) Spins," *Chem. Phys. Lett.*, **1996,** *262*, 737–743.
100. P. T. Callaghan, M. A. Le Gros, and D. N. Pinder, "The Measurement of Diffusion Using Deuterium Pulsed Gradient Nuclear Magnetic Resonance," *J. Chem. Phys.*, **1983,** *79*, 6372–6381.
101. I. Furo and B. Halle, "2D Quadrupolar-Echo Spectroscopy with Coherence Selection and Optimized Pulse Angle," *J. Magn. Reson.*, **1992,** *98*, 388–407.
102. M. Holz and H. Weingärtner, "Calibration in Accurate Spin-Echo Self-Diffusion Measurements Using ^{1}H and Less-Common Nuclei," *J. Magn. Reson.*, **1991,** *92*, 115–125.
103. D. W. McCall, D. C. Douglass, and E. W. Anderson, "Self-Diffusion Studies by Means of Nuclear Magnetic Resonance Spin-Echo Techniques," *Ber. Bunsenges. Phys. Chem.*, **1963,** *67*, 336–340.
104. I. S. Gradshteyn and I. M. Ryzhik, *Table of Integrals, Series, and Products*, Academic, New York, 1994.
105. A. P. Prudnikov, Y. A. Brychkov, and O. I. Marichev, *Elementary Functions*, Gordon and Breach, New York, 1990.
106. J. S. Murday, "Measurement of Magnetic Field Gradient by Its Effect on the NMR Free Induction Decay," *J. Magn. Reson.*, **1973,** *10*, 111–120.
107. R. L. Vold, R. R. Vold, and H. E. Simon, "Errors in Measurements of Transverse Relaxation Rates," *J. Magn. Reson.*, **1973,** *11*, 283–298.
108. E. Fukushima, A. A. V. Gibson, and T. A. Scott, "Carbon-13 NMR of Carbon Monoxide. II. Molecular Diffusion and Spin-Rotation Interaction in Liquid CO," *J. Chem. Phys.*, **1979,** *71*, 1531–1536.
109. E. Fukushima and S. B. W. Roeder, *Experimental Pulse NMR: A Nuts and Bolts Approach*, Addison-Wesley, London, 1981.
110. D. M. Lamb, P. J. Grandinetti, and J. Jonas, "Fixed Field Gradient NMR Diffusion Measure-

ments Using Bessel Function Fits to the Spin-Echo Signal," *J. Magn. Reson.*, **1987,** *72*, 532–539.
111. M. I. Hrovat and C. G. Wade, "Absolute Measurements of Diffusion Coefficients by Pulsed Nuclear Magnetic Resonance," *J. Chem. Phys.*, **1980,** *73*, 2509–2510.
112. P. J. Basser, J. Mattiello, and D. Le Bihan, "Estimation of the Effective Self-Diffusion Tensor from the NMR Spin Echo," *J. Magn. Reson.*, **1994,** *B103*, 247–254.
113. W. S. Price, K. Hayamizu, and Y. Arata, "Optimization of the Water-PRESS Pulse Sequence and Its Integration into Pulse Sequences for Studying Biological Molecules," *J. Magn. Reson.*, **1997,** *126*, 256–265.
114. A. S. Altieri, D. P. Hinton, and R. A. Byrd, "Association of Biomolecular Systems via Pulsed Field Gradient NMR Self-diffusion Measurements," *J. Am. Chem. Soc.*, **1995,** *117*, 7566–7567.
115. P. C. M. Van Zijl and C. T. W. Moonen, "Complete Water Suppression for Solutions of Large Molecules Based on Diffusional Differences between Solute and Solvent (DRYCLEAN)," *J. Magn. Reson.*, **1990,** *87*, 18–25.
116. E. D. von Meerwall and R. D. Ferguson, "A Fortran Program to Fit Diffusion Models to Field-Gradient Spin Echo Data," *Comput. Phys. Commun.*, **1981,** *21*, 421–429.
117. M. S. Crawford, B. C. Gerstein, A.-L. Kuo, and C. G. Wade, "Diffusion in Rigid Bilayer Membranes: Use of Combined Multiple Pulse and Multiple Pulse Gradient Techniques in Nuclear Magnetic Resonance," *J. Am. Chem. Soc.*, **1980,** *102*, 3728–3732.
118. A. F. Collings and R. Mills, "Temperature-Dependence of Self-Diffusion for Benzene and Carbon Tetrachloride," *J. Chem. Soc. Faraday Trans.*, **1970,** *66*, 2761–2766.
119. H. Weingärtner, "Self-diffusion in Liquid Water: A Reassessment," *Z. Phys. Chem.*, **1982,** *132*, 129–149.
120. R. Mills, "Self-diffusion in Normal and Heavy Water in the Range 1–45 Degrees," *J. Phys. Chem.*, **1973,** *77*, 685–688.
121. M. Holz, R. Haselmeier, R. K. Mazitov, and H. Weingärtner, "Self-diffusion of Neon in Water by ^{21}Ne NMR," *J. Am. Chem. Soc.*, **1994,** *116*, 801–802.
122. R. Mills and V. V. M. Lobo, *Self-diffusion in Electrolyte Solutions*, Elsevier, Amsterdam, 1989.
123. H. Weingärtner, R. Haselmeier, and M. Holz, "^{129}Xe NMR As a New Tool for Studying Gas Diffusion in Liquids: Self-diffusion of Xenon in Water," *Chem. Phys. Lett.*, **1992,** *195*, 596–601.
124. W. S. Price, "Probing Molecular Dynamics in Biochemical and Chemical Systems Using Pulsed Field Gradient NMR Diffusion Measurements," in *Recent Advances in Analytical Techniques*, Atta-Ur-Rahman, Ed., Gordon and Breach, Amsterdam, 1998.
125. W. S. Price, B. E. Chapman, B. A. Cornell, and P. W. Kuchel, "Translational Diffusion of Glycine in Erythrocytes Measured at High Resolution with Pulsed Field Gradients," *J. Magn. Reson.*, **1989,** *83*, 160–166.
126. W. S. Price, B. E. Chapman, and P. W. Kuchel, "Correlation of Viscosity and Conductance with $^{23}Na^+$ NMR T_1 Measurements," *Bull. Chem. Soc. Jpn.*, **1990,** *63*, 2961–2965.
127. W. S. Price, M. Nara, and Y. Arata, "A Pulsed Field Gradient NMR Study of the Aggregation and Hydration of Parvalbumin," *Biophys. Chem.*, **1997,** *65*, 179–187.
128. A. J. Dingley, J. P. Mackay, B. E. Chapman, M. B. Morris, P. W. Kuchel, B. D. Hambly, and G. F. King, "Measuring Protein Self-association using Pulsed-Field-Gradient NMR Spectroscopy: Application to Myosin Light Chain 2," *J. Biomol. NMR*, **1995,** *6*, 321–328.
129. V. V. Krishnan, "Determination of Oligomeric State of Proteins in Solution from Pulsed-Field-Gradient Self-Diffusion Coefficient Measurements: A Comparison of Experimental, Theoretical, and Hard-Sphere Approximated Values," *J. Magn. Reson.*, **1997,** *124*, 468–473.

William S. Price received his B.Sc. and Ph.D. (Biochemistry) degrees from the University of Sydney in 1986 and 1990, respectively. His Ph.D. studies were under the supervision of Professor Philip W. Kuchel and Dr. Bruce A. Cornell. He did postdoctoral study at the Institute of Atomic and Molecular Science in Taipei, Taiwan (1990–1993) with Professor Lian-Pin Hwang and at the National Institute of Material and Chemical Research in Tsukuba, Japan (1993–1995) with Dr. Kikuko Hayamizu. In 1995 he joined the research staff at the Water Research Institute in Tsukuba, Japan and presently holds the position of Chief Scientist. His interests focus on the use of NMR techniques such as pulsed-field gradient NMR, NMR microscopy, spin relaxation, and solid-state ^{2}H-NMR to study molecular dynamics in chemical and biochemical systems.